iScience

Article

An integrative proteomics approach identifies tyrosine kinase KIT as a therapeutic target for SPINK1-positive prostate cancer

Nishat Manzar, Umar Khalid Khan, Ayush Goel, Shannon Carskadon, Nilesh Gupta, Nallasivam Palanisamy, Bushra Ateeq

bushra@iitk.ac.in

Highlights

SPINK1 activates KIT receptor tyrosine kinase signaling in prostate cancer

Targeting KIT signaling attenuates SPINK1-mediated oncogenicity and stemness

KIT signaling transactivates β-catenin and interferes with AR

Inhibition of KIT signaling attenuates prostate tumor growth and metastases

Article

An integrative proteomics approach identifies tyrosine kinase KIT as a therapeutic target for SPINK1-positive prostate cancer

Nishat Manzar,[1] Umar Khalid Khan,[1] Ayush Goel,[1] Shannon Carskadon,[2] Nilesh Gupta,[3] Nallasivam Palanisamy,[2] and Bushra Ateeq[1,4,5,6,*]

SUMMARY

Elevated serine peptidase inhibitor, Kazal type 1 (SPINK1) levels in ∼10%–25% of prostate cancer (PCa) patients associate with aggressive phenotype, for which there are limited treatment choices and dismal clinical outcomes. Using an integrative proteomics approach involving label-free phosphoproteome and proteome profiling, we delineated the downstream signaling pathways involved in SPINK1-mediated tumorigenesis and identified tyrosine kinase KIT as highly enriched. Furthermore, high to moderate levels of KIT expression were detected in ∼85% of SPINK1-positive PCa specimens. We show KIT signaling orchestrates SPINK1-mediated oncogenesis, and treatment with KIT inhibitor reduces tumor growth and metastases in preclinical mice models. Mechanistically, KIT signaling modulates WNT/β-catenin pathway and confers stemness-related features in PCa. Notably, inhibiting KIT signaling led to restoration of AR/REST levels, forming a feedback loop enabling SPINK1 repression. Overall, we uncover the role of KIT signaling downstream of SPINK1 in maintaining lineage plasticity and provide distinct treatment modalities for advanced-stage SPINK1-positive patients.

INTRODUCTION

Therapy resistance allied with disease recurrence is a pervasive problem in prostate cancer (PCa) patients. The standard of care for localized disease often involves surgical castration and/or androgen deprivation therapy (ADT).[1] Of these, majority of patients at some time point experience tumor relapse, leading to the emergence of castration-resistant prostate cancer (CRPC).[2,3] Nearly one-fifth of metastatic CRPC patients succumb to small-cell neuroendocrine prostate cancer (NEPC) due to ADT-mediated lineage crisis.[4,5] Earlier, we have shown that AR antagonists led to the upregulation of SPINK1 and genes associated with NEPC in CRPC mice models as well as in patients who underwent neoadjuvant hormone therapy.[6] The survival rate of these patients is less than a year, primarily due to its aggressiveness and limited treatment options.[7]

High levels of serine peptidase inhibitor, Kazal type 1 (SPINK1) represent the second-largest molecular subtype (∼10%–25%) of PCa, associated with shorter biochemical recurrence and rapid progression to castration resistance.[8–11] SPINK1, being a small secretory protein, acts in an autocrine/paracrine manner to promote tumor progression.[12,13] Furthermore, it has been linked with gastrointestinal-lineage signature genes aberrantly expressed in ∼30% of the CRPC cases owing to the activation of hepatocyte nuclear factors' (HNF4G/HNF1A) transcriptional circuitry.[14] In addition, genotoxic chemotherapy is known to trigger SPINK1 expression in the stromal cells, thereby promoting therapy resistance.[15] Recently, we demonstrated that the androgen receptor (AR) and RE1-silencing transcription factor (REST) function as transcriptional repressors of *SPINK1*, and AR antagonists release this repression, resulting in its upregulation.[6] Taken together, considering the functional significance of SPINK1 in PCa, there is a need to uncover its downstream unidentified signaling pathways, which may lead to the development of unconventional therapeutic strategies for this aggressive subtype.

Here, we delineate the downstream signaling pathways involved in SPINK1-mediated tumorigenicity by integrating the label-free phosphoproteome and proteome profiling data of SPINK1-positive PCa cells. Of all the enriched receptor tyrosine kinases, KIT receptor tyrosine kinase exhibits higher expression in NEPC compared with CRPC specimens. Additionally, we also examined KIT levels in PCa specimens, and ∼85% of SPINK1-positive PCa patients display high to moderate levels of KIT expression. We decipher that KIT signaling plays a crucial role in modulating the WNT/β-catenin pathway, and its inhibition restores the AR and REST levels, forming a feedback loop resulting in SPINK1 repression. Importantly, pharmacological inhibition of KIT resulted in the abrogation of oncogenic properties specifically associated with

[1]Molecular Oncology Laboratory, Department of Biological Sciences and Bioengineering, Indian Institute of Technology Kanpur, Kanpur, UP 208016, India
[2]Vattikuti Urology Institute, Department of Urology, Henry Ford Health System, Detroit, MI 48202, USA
[3]Department of Pathology, Henry Ford Health System, Detroit, MI 48202, USA
[4]Mehta Family Center for Engineering in Medicine, Indian Institute of Technology Kanpur, Kanpur, UP 208016, India
[5]Centre of Excellence for Cancer - Gangwal School of Medical Sciences and Technology, Indian Institute of Technology Kanpur, Kanpur, UP 208016, India
[6]Lead contact
*Correspondence: bushra@iitk.ac.in
https://doi.org/10.1016/j.isci.2024.108794
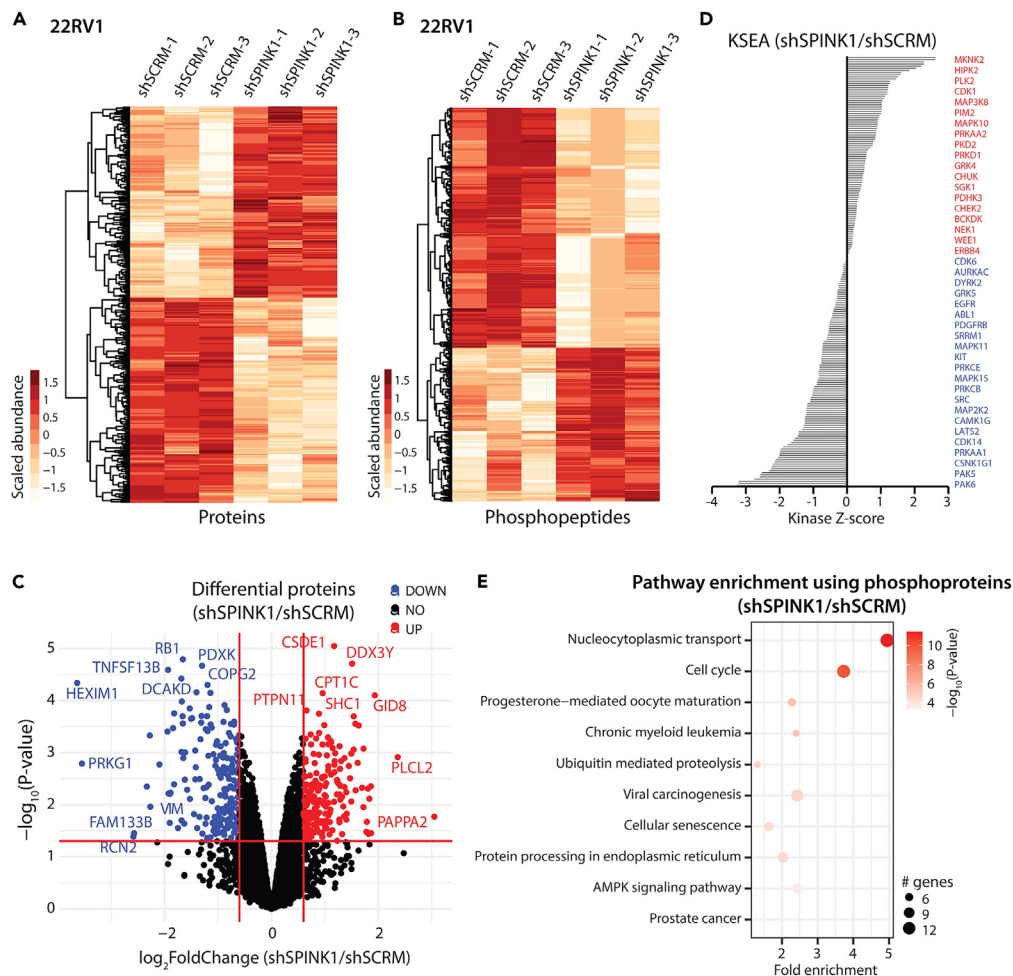
Figure 1. Global quantitative proteome and phosphoproteome profiling of the SPINK1-knockdown prostate cancer cells

(A) Heatmap depicting the Z-scaled abundance of significant proteins in 22RV1-shSCRM and 22RV1-shSPINK1 cells.

(B) Same as in (A), except for significantly enriched phosphoproteins in 22RV1-shSCRM and 22RV1-shSPINK1 cells. Each sample was analyzed in biological triplicates.

(C) Volcano plot showing the differentially enriched proteins in 22RV1-shSPINK1 versus 22RV1-shSCRM cells; blue dots are downregulated, and red dots are upregulated proteins in shSPINK1, whereas black dots signify no change.

(D) Kinase-substrate enrichment analysis of the phosphopeptides enriched in 22RV1-shSPINK1 versus 22RV1-shSCRM cells. Identified kinases are plotted with their respective Z scores; blue kinases have negative Z score, and red kinases have positive Z score in 22RV1-shSPINK1 versus 22RV1-shSCRM cells. A negative Z score corresponds to a collective dephosphorylation of the kinase's substrates; the inverse is true for a positive score.

(E) Pathway enrichment analysis for differential phosphoproteins in 22RV1-shSPINK1 versus 22RV1-shSCRM cells using pathfindR; size of the dot represents number of genes, and the color symbolizes the -log$_{10}$(p value) of the enriched pathway. See also Figure S1 and S2.

stemness phenotype, accompanied by reduced tumor growth and metastases. Collectively, we uncover the role of KIT signaling downstream of SPINK1, thus reinforcing its significance in modulating lineage plasticity and PCa progression.

RESULTS

Global proteome and phosphoproteome profiling of SPINK1-positive prostate cancer

Dysregulated phosphorylation of proteins perturbs the activity of several biological pathways, leading to tumorigenesis and metastases.[16] Integrated proteomics studies offer an in-depth comprehension of cancer pathobiology and could untangle its complex circuitries. To decipher the signaling involved in SPINK1-mediated tumorigenesis, we performed label-free quantitative proteome and phosphoproteome profiling of small-hairpin RNA-mediated *SPINK1* silenced (shSPINK1) and control small-hairpin RNA scrambled (shSCRM) 22RV1 cells (Figure S1). Our integrated proteomics data revealed ~4,000 proteins and enriched ~6,000 phosphopeptides in each biological replicate. Of these, 367 proteins and 807 phosphopeptides were found to be significantly altered between shSCRM and shSPINK1 cells (Figures 1A and 1B). The differential enrichment analysis led to the identification of 190 downregulated proteins and 177 upregulated proteins (Figure 1C).
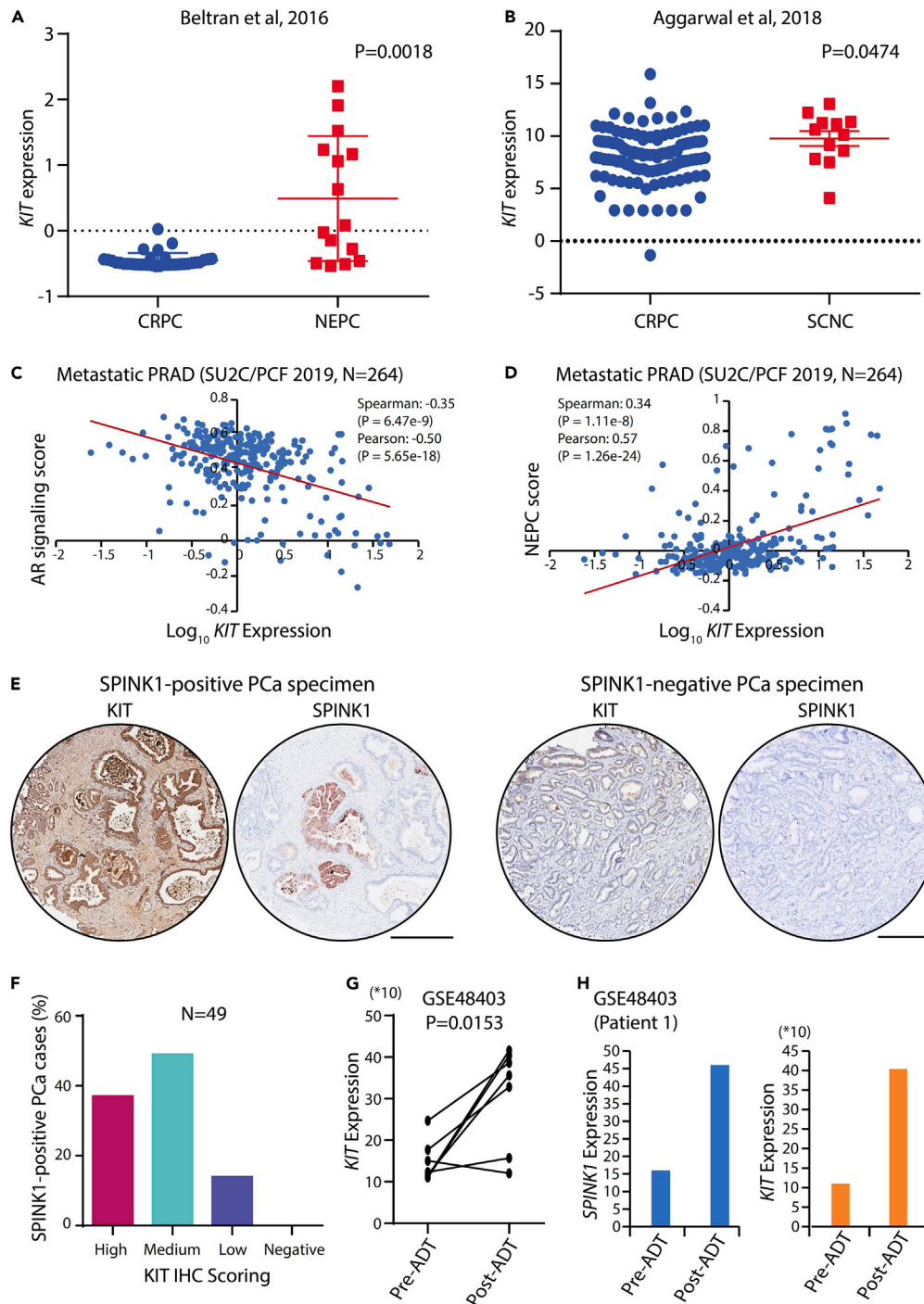
Figure 2. KIT tyrosine kinase is highly expressed in androgen-independent prostatic tumors

(A) *KIT* mRNA expression in Beltran et al., 2016 dataset. p value was calculated using Unpaired Student's t test with Welch's correction.

(B) Same as (A), except for Aggarwal et al., 2018 dataset.

(C) Scatterplot showing correlation of *KIT* mRNA expression (FPKM polyA) [$\log_{10}$(value + 1)] with AR signaling score in metastatic prostate adenocarcinoma (SU2C/PCF 2019) dataset. Coefficient values for both Spearman and Pearson correlation along with the p value are depicted in the plot.

(D) Same as in (C), except for the correlation of *KIT* mRNA expression with NEPC score.

Figure 2. Continued

(E) Micrographs representing immunohistochemical (IHC) staining for KIT and SPINK1 expression in tissue microarrays of prostate cancer specimens, SPINK1-positive patient (left) and SPINK1-negative patient (right). Scale bar represents 300 μm.

(F) Bar plot depicting the percentage of SPINK1-positive patients' specimens for KIT intensity (high/medium/low/negative).

(G) Dot plot showing *KIT* expression in PCa patients with or without ADT, GSE48403. Statistical significance was calculated using paired t test.

(H) Bar plots showing *SPINK1* and *KIT* expression in 22 weeks ADT-treated PCa patient with Gleason score 8 and TNM stage 3b. See also Figure S3 and S4.

Also, 492 downregulated phosphopeptides and 315 upregulated phosphopeptides were noted in 22RV1-shSPINK1 versus 22RV1-shSCRM cells (Figure S2A). Because deregulated kinases have been associated with cancer, and kinase-targeting drug such as imatinib has been a great success in multiple cancer types,[17,18] we examined the kinases involved in this differential phosphorylation of proteins using kinase-substrate enrichment analysis (KSEA).[19] We identified ~200 kinases to be enriched in the kinase-substrate relationship, and decreased activity of 108 kinases, including MET, CSF1R, FLT3, KIT, INSR, PDGFRB, ERBB2, and EGFR, was noticed in SPINK1-ablated cells relative to the control (Figure 1D). Furthermore, to identify the biological pathways governed by the dysregulated proteins and phosphopeptides, we performed pathway enrichment analysis using pathfindR and DAVID functional annotation tools.[20,21] Notably, cell cycle, ubiquitin-mediated proteolysis, protein processing in endoplasmic reticulum, AMPK signaling, and PCa appeared as few of the top ten significantly altered pathways with SPINK1 silencing (Figures 1E, S2B, and S2C). These findings reveal that SPINK1 engages distinct kinases to direct the activation or deactivation of downstream signaling pathways in promoting tumorigenesis and stemness in PCa.

Sustained receptor tyrosine kinase KIT signaling and SPINK1 drive neuroendocrine prostate cancer

ADT-induced SPINK1 plays a crucial role in governing stemness as well as in the maintenance of neuroendocrine phenotype.[6] To explore the SPINK1-activated receptor tyrosine kinase in advanced-stage PCa, we examined the expression of different kinases in publicly available NEPC datasets (Figures 2A and S3A–S3G). Interestingly, higher expression of *KIT* and *INSR* kinases in NEPC (N = 15) compared with CRPC specimens (N = 34) was observed in the Beltran cohort (Figures 2A and S3G). Similarly, high expression of *KIT* was noted in small-cell NEPC (SCNC) (N = 12) compared with metastatic CRPC (N = 107) specimens in the Aggarwal et al. dataset[4] (Figure 2B). However, no significant change in *INSR* expression between metastatic CRPC and small-cell NEPC specimens was detected in Aggarwal et al. dataset (Figure S3H). Next, to examine a plausible link between KIT and androgen signaling, we analyzed the association of *KIT* and AR signaling scores in the metastatic prostate adenocarcinoma (SU2C/PCF Dream Team) cohort (N = 264). Like *SPINK1* expression, *KIT* also displayed an inverse association with AR signaling (Figures 2C and S4A). Additionally, a positive correlation between *KIT* and NEPC gene signature was seen in metastatic CRPC, concurring with a positive association of SPINK1 and NEPC score (Figures 2D and S4B). Notably, no significant association of INSR with either AR signaling or NEPC score was detected in CRPC specimens (Figures S4C and S4D). Next, we performed immunohistochemical (IHC) staining for the expression of KIT and SPINK1 in the tissue microarray (TMA) and found that ~85% of SPINK1-positive PCa specimens (N = 49) exhibited high to medium levels of KIT expression (Figures 2E, 2F, and S4E). Subsequently, we examined the *SPINK1* and *KIT* expression in NEPC patient-derived organoids (GSE112786) and found higher levels of *KIT* in SPINK1-positive NEPC organoids, corroborating with our cell lines data (Figure S4F). We also checked *SPINK1* and *KIT* expression in advanced PCa specimens who underwent ADT for ~22 weeks (GSE48403) and noticed high levels of *SPINK1* and *KIT* in post-ADT patients' specimens relative to pre-ADT (Figures 2G, 2H, and S4G). Collectively, these results highlight the association of receptor tyrosine kinase KIT signaling and SPINK1 in androgen-independent prostatic tumors.

Pharmacological inhibition of KIT signaling perturbs SPINK1-mediated tumorigenesis

Having established the connection between receptor tyrosine kinase KIT signaling and SPINK1, we determined the protein level expression of KIT and SPINK1 across different PCa and benign prostate epithelial cells. To our interest, both the proteins exhibited high expression in NCIH660, an epithelial neuroendocrine cell line, followed by a moderate expression in 22RV1, a castrate-resistant cell line (Figures S5A and S5B). Next, we sought to examine the effect of recombinant SPINK1 (rSPINK1) on KIT signaling and found that stimulation of 22RV1 cells with rSPINK1 leads to an increase in the KIT Y703 phosphorylation in a time-dependent manner (Figure 3A). Moreover, we performed pharmacological inhibition of KIT using pexidartinib (KITi) and evaluated its impact on SPINK1-mediated tumorigenesis. A significant decrease in cell proliferation and viability was observed in KITi-treated 22RV1 cells compared with control (Figures 3B and S5C).

Further, to investigate the effect of KIT signaling inhibition in therapy-resistant PCa, the expression of *SPINK1* and *KIT* was first examined in 16D^CRPC treated with enzalutamide for 10 days and enzalutamide-resistant 42D^ENZR cells (GSE183199).[22] Notably, an increase in *SPINK1* expression in castrate-resistant 16D^CRPC was observed, whereas in enzalutamide-resistant 42D^ENZR cells, both *SPINK1* and *KIT* were elevated (Figure S5D). Moreover, marked reduction in cell proliferation and viability of 42D^ENZR cells with increasing concentrations of KITi was noted (Figures 3C and S5E). Notably, half-maximal inhibitory concentration (IC50) of KITi for 22RV1 cells was 16.9 μM with ~50% reduction in cell viability (Figure S5F). To examine the effect of KIT kinase in anchorage-independent growth, foci formation ability of 22RV1 cells was performed in presence and absence of KITi, and ~90% reduction in the foci formation ability was noticed with a sub-IC50 concentration (10 μM) of KITi (Figure 3D). Alongside, KITi (10 μM) treatment also led to a robust decrease in the foci formation ability of 42D^ENZR cells (Figure 3E), supporting the probable function of KIT signaling in imparting therapy resistance in conjunction with high SPINK1 levels.

To evaluate the significance of KIT signaling in conferring stemness and self-renewal capacity, tumorsphere formation assay was performed, and ~70%–80% reduction in tumorsphere formation efficiency and mean area of 22RV1 tumorspheres treated with KITi was noted compared with control (Figure 3F). Furthermore, we also performed siRNA-mediated *KIT* silencing in 22RV1 cells, and a marked reduction in
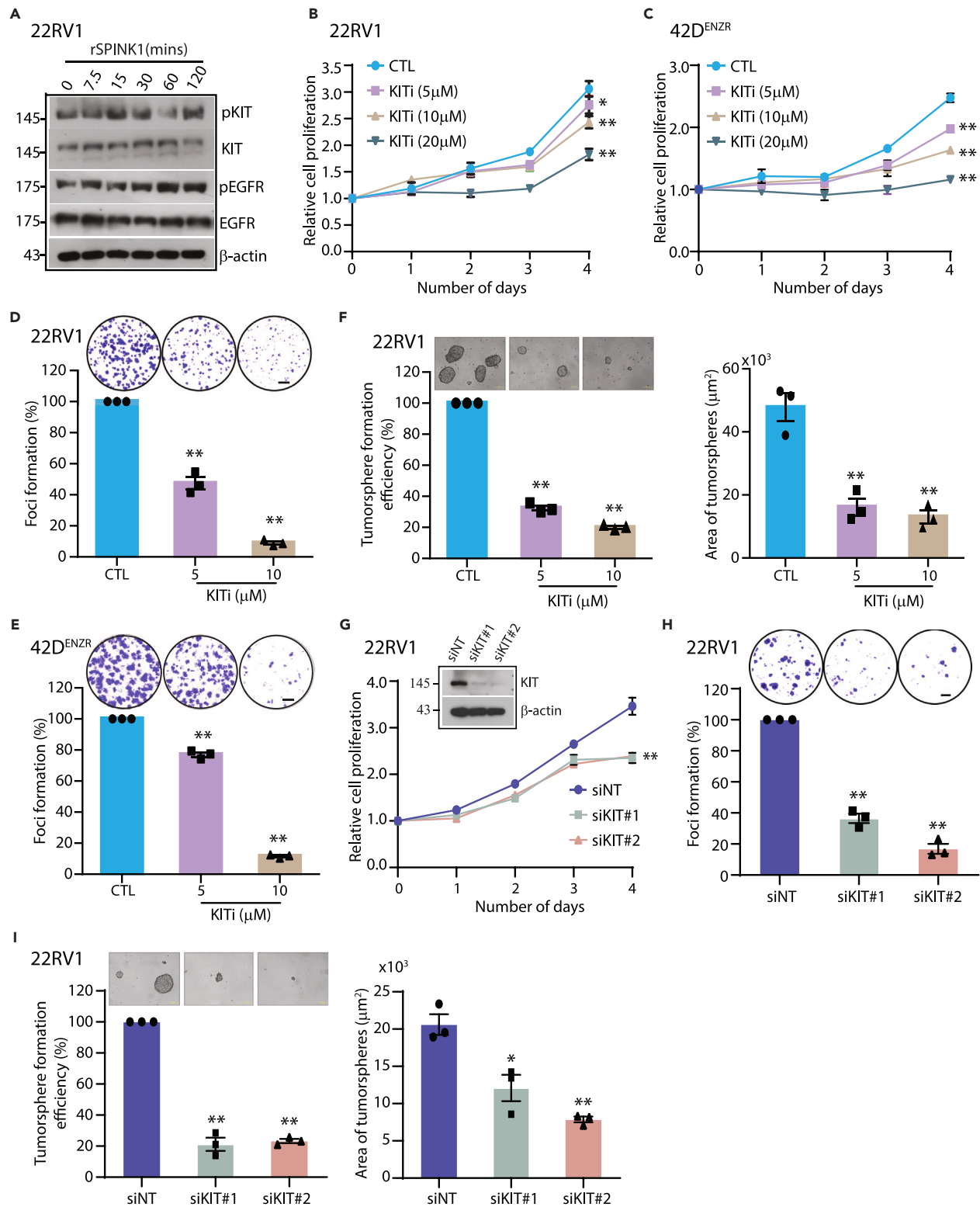
Figure 3. KIT tyrosine kinase inhibition attenuates oncogenic characteristics

(A) Immunoblot showing phospho-KIT (Y703), KIT, phospho-EGFR (Y845), and EGFR levels in 22RV1 cells stimulated with recombinant SPINK1 (100 ng/mL) at different time points. β-actin was used as the loading control.

(B) Line plot representing relative cell proliferation of 22RV1 cells along with different concentrations of KIT tyrosine kinase inhibitor, KITi, and control (CTL).

Figure 3. *Continued*

(C) Same as in (B), except for 42D^ENZR cells.

(D) Representative images for foci of 22RV1 cells in the respective conditions (top). Bar plot showing percent foci formation efficiency of 22RV1 cells treated with indicated concentrations of KITi and CTL. Scale bar represents 1,000 μm.

(E) Same as in (D), except for 42D^ENZR cells.

(F) Representative images (top) and bar plots showing percent tumorsphere formation efficiency (left) and mean area of 22RV1 tumorspheres (right) treated with indicated concentrations of KITi and CTL. Scale bar represents 100 μm.

(G) Immunoblot showing KIT levels in *KIT*-silenced 22RV1 cells. β-actin was used as the loading control (top). Same as in (B), except for *KIT*-silenced 22RV1 cells (bottom).

(H) Same as in (D), except for *KIT*-silenced 22RV1 cells.

(I) Same as in (F), except for *KIT*-silenced 22RV1 cells. Each experiment was performed in biological triplicates (N = 3); the bar represents mean ± SEM, and each dot represents individual value. Statistical significance was calculated using two-way or one-way ANOVA followed by Dunnett's multiple comparison test. p value: *<0.05 and **<0.01. See also Figure S5.

cell proliferation, viability, foci, and tumorsphere-forming abilities was noted (Figures 3G–3I and S5G). Collectively, these findings suggest the central role of KIT signaling in governing oncogenic attributes associated with SPINK1 in PCa.

Pharmacological inhibition of KIT signaling mitigates SPINK1-mediated cancer stemness

KIT has been characterized as one of the important markers of prostate stem cells and is known to play a key role in the organogenesis of prostate gland.[23] In PCa, KIT is known to drive disease aggressivity through the cancer stem-like cells (CSCs) phenotype and resistance to tyrosine kinase inhibitor.[24] To evaluate the role of KIT signaling in maintaining cancer-associated stemness, RNA was isolated from the tumorspheres generated in Figure 3F. The expression of markers associated with cellular reprogramming was examined, and a notable decrease in the expression of *MYC*, *OCT4*, *SOX2*, *TET1*, and *AURKA* was noticed in KITi-treated tumorspheres and 22RV1 cells compared with control (Figures 4A and S6A).

Furthermore, KITi-treated tumorspheres and 22RV1 cells showed a robust decrease in the expression of stem cell surface markers, namely, *CD24*, *CD44*, and *KIT/CD117* (Figures 4B and S6B). In agreement with tumorsphere data, a similar trend of reduced expression of stemness-related markers in KITi-treated and *KIT*-silenced 42D^ENZR cells was noticed (Figures 4C and 4D). To consolidate the changes at the gene expression level of cell surface stem cell markers, we also examined the localization and surface expression of CD44, and ~75% reduction in the cell surface levels of CD44 was recorded upon treatment with KITi compared with control (Figures 4E and 4F). In addition, KIT signaling inhibition in long-term androgen-deprived LNCaP cells (LNCaP-AI), which express high SPINK1, also demonstrated a modest decrease in the expression of stem cell surface markers (Figures S6C and S6D). These findings emphasize the role of KIT signaling in maintaining stemness in the context of SPINK1-positive cancers.

Inhibition of KIT diminished SPINK1-mediated osteolytic bone metastases

The role of KIT signaling has been well defined in the progression of gastrointestinal stromal tumors[25]; however, its allies in prostate tumorigenesis remain elusive. To address this question, we generated doxycycline (Dox)-inducible KIT overexpressing 22RV1 cells, namely, 22RV1-KIT (Figure S7A), and KIT signaling inhibition via a decrease in phosphorylation levels of KIT using KITi was confirmed (Figure 5A). To identify the KIT interacting partners, we performed immunoprecipitation coupled with tandem mass spectrometry (IP-MS) and identified 306 proteins exclusive to KIT pull-down assay (Figure 5B). Poly [ADP-ribose] polymerase 1 (PARP-1), histones, heterogeneous nuclear ribonucleoproteins (hnRNPs), the 40S and 60S ribosomal proteins (40S/60S RPs), and proteasome subunit α and β (PSMAs/PSMBs) were some of the proteins enriched in KIT IP-MS (Figure 5B; Table S1). Biological processes enrichment using KIT-interacting partners (N = 306) discovered multiple significant pathways (Figure 5C). Surprisingly, most of these processes regulated by KIT interactome show similarity to the processes associated with SPINK1-downregulated proteins, for instance, translation, mRNA processing, and RNA splicing (Figure S7B). Furthermore, 33 proteins were shared among KIT-interacting proteins and SPINK1-downregulated proteins, whereas 19 proteins were seen as common between KIT interactome and SPINK1-upregulated proteins (Figure S7C). These findings imply the involvement of KIT signaling in the regulation of biological processes, such as mRNA processing, splicing, and translation in SPINK1-positive PCa.

Interestingly, KIT interactome pathway analysis highlighted osteoblast differentiation as one of the significant biological processes (Figure 5C). In analogy, KIT is constitutively expressed on the human osteoclasts and plays key role in bone resorption and remodeling.[26] Because 22RV1 tumors-associated bone metastases demonstrate both osteolytic and osteoblastic features,[27,28] we aimed to examine the effect of KIT signaling using an experimental bone metastasis model. Toward this, 22RV1 cells were implanted via intramedullary injection in the tibia of NOD/SCID mice and administered them with KITi (pexidartinib, 50 mg/kg) or vehicle control (CTL) orally for three weeks. Bone metastases in the tibiae were monitored by x-ray, and the characteristics and extent of bone lesions were examined by micro-computed tomography (μCT) (Figures S8A, S8B, and 5D). Notably, a significant increase in the number of trabeculae suggestive of more cancellous bone remodeling was observed in the mice treated with KITi (Figures 5D and 5E). Furthermore, assessment of the proximal epiphysis and metaphysis regions revealed moderate changes in the bone morphometric parameters, such as bone surface density and bone surface/volume ratio with KIT inhibition (Figure 5E). These findings employ the role of KIT signaling in osteolytic PCa bone metastases.
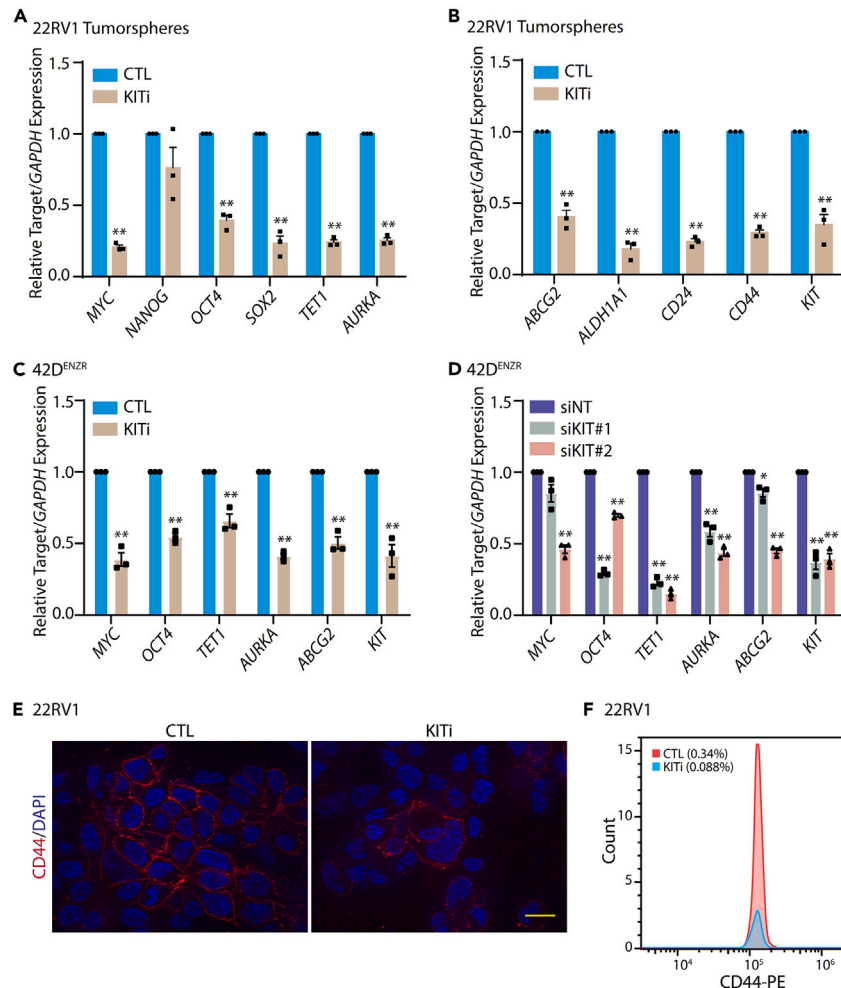
Figure 4. KIT tyrosine kinase inhibition mitigates stemness-related features

(A) Bar plot showing quantitative PCR (qPCR) data for the relative expression of stemness-associated genes in KITi (10 µM)/CTL-treated 22RV1 tumorspheres.

(B) Same as in (A), except for relative expression of stem cell surface markers. (C) Same as in (A), except for KITi/CTL-treated 42D^ENZR cells.

(D) Same as (C), except for KIT-silenced 22RV1 cells.

(E) Micrographs representing immunostaining for CD44 in KITi/CTL-treated 22RV1 cells. Scale bar represents 10 µm.

(F) Histogram depicting flow cytometry analysis of CD44 staining in KITi/CTL-treated 22RV1 cells. Each experiment was performed in biological triplicates (N = 3); the bar represents mean ± SEM, and each dot represents individual value. Statistical significance was calculated using two-way ANOVA followed by Sidak's multiple comparison test. p value: *<0.05 and **<0.01. See also Figure S6.

Targeting KIT signaling restores AR/REST axis by impairing WNT signaling

The CD44 stem cell marker has long been defined as a target of WNT/β-catenin pathway in the intestinal tumorigenesis.[29] In our IP-MS data, KIT showed direct interaction with β-catenin with nine peptide spectral matches (Table S1). Also, KIT signaling inhibition resulted in diminished stemness and reduced CD44 levels (Figures 4E and 4F); therefore, we conjectured its effect on WNT/β-catenin pathway. Notably, a rampant decrease in the expression of genes associated with WNT signaling, such as *CTNNB1*, *TCF7L2*, *SOX9*, and *AXIN2*, was found in KITi-treated 22RV1 tumorspheres as well as cells (Figures 6A and S9A). Similar results were obtained in enzalutamide-resistant 42D^ENZR and androgen-deprived LNCaP-AI cells treated with KITi (Figures 6B and S9B). Likewise, KITi treatment and siRNA-mediated *KIT* silencing ensued a marked decrease in the protein levels of β-catenin, CD44, and KIT relative to the control (Figures 6C and 6D). In contrast, inducible KIT overexpression in 22RV1 cells demonstrated high levels of β-catenin compared with the control (Figure 6E). Moreover, analyzing publicly available single-cell RNA-seq data (OMIX001928) for NEPC transgenic mice indicates robust interaction between KIT and WNT signaling in the neuroendocrine cells (Figure S9C), signifying that KIT signaling regulates stemness-associated β-catenin pathway in prostate tumorigenesis. Furthermore, KITi treatment led to reduced phosphorylation of ERK and AKT (Figure S9D), which is a prototypic readout of KIT tyrosine kinase inhibition. On another note, the PI3K-Akt signaling pathway is known to harness ubiquitin-mediated proteasomal pathway to degrade AR.[30] Interestingly, "ubiquitin mediated proteolysis" and "proteasomal protein catabolic process" showed up as the top significant pathways
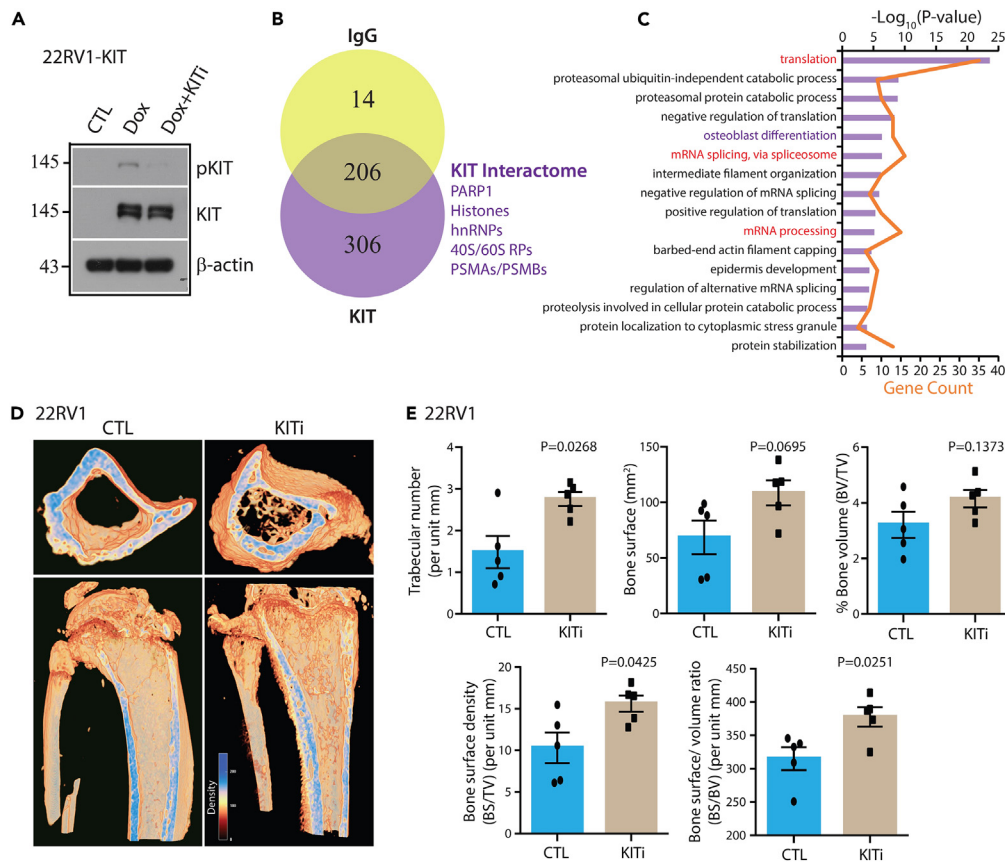
Figure 5. KIT tyrosine kinase inhibition limits metastatic bone lesions

(A) Immunoblot showing phosphorylated-KIT (pKIT) and KIT levels in 22RV1-KIT cells induced with doxycycline (Dox) and treated with KITi. β-actin was used as the loading control.

(B) Venn diagram depicting common and specific proteins between immunoglobulin G (IgG) and KIT pull-down in Dox-induced 22RV1-KIT cells. A few KIT interacting partners are also labeled.

(C) DAVID functional annotation analysis showing enriched biological processes using KIT interactome (N = 306). The bar denotes -log$_{10}$(p value), and the line represents gene count.

(D) Micrographs representing micro-CT analysis of proximal horizontal (top) and longitudinal cross-sectional view (bottom) of the tibiae from mice with 22RV1 intratibial implantation and administered with KITi (50 mg/kg)/CTL via oral gavage (each group, N = 5).

(E) Bar plots showing bone morphometric parameters in the tibiae, same as shown in (D). Bar represents mean ± SEM, and each dot represents the individual value. Statistical significance was calculated using unpaired Student's t test with Welch's correction. p value: *<0.05 and **<0.01. See also Figure S7 and S8 and Table S1.

enriched in the SPINK1-regulated phosphoproteins and KIT-interacting proteins (Figures 1E and 5C). Taking cues from these results, we interrogated the effect of KIT signaling inhibition on the AR levels, and a concentration-dependent rise in AR and its corepressor REST levels was observed upon KITi treatment (Figure 6F). Moreover, KITi treatment or RNAi-mediated *KIT* silencing led to a decrease in the SPINK1 levels (Figures 6F and 6G), possibly due to increased levels of AR and its co-repressor REST, as shown previously.[6] Similarly, KIT signaling inhibition led to AR/REST restoration in LNCaP-AI cells, which in turn hampered neuroendocrine phenotype marked by a decrease in the β3-tubulin levels (Figure 6H). Moreover, a remarkable reduction in markers associated with NEPC (*ENO2, CHGA, CD56,* and *NMYC*) and REST target genes (*SYN1* and *BDNF*) was noted in KITi-treated 22RV1, 42D^{ENZR}, and LNCaP-AI cells (Figures 6I and S9E–S9G). Also, KIT signaling inhibition showed a decrease in the *NCAD,* a mesenchymal marker, along with a modest increase in the *ECAD,* an epithelial marker (Figure S9E), suggesting its role in cellular plasticity. Collectively, these results lay down a distinctive mechanism wherein KIT signaling regulates the stability of AR and REST, which in turn governs the SPINK1-positive PCa transition to neuroendocrine phenotype.

Pharmacological inhibition of KIT signaling attenuates tumor growth and metastases

To understand the therapeutic utility of KIT inhibitor in SPINK1-mediated PCa progression, 22RV1 cells were subcutaneously implanted in the flank region of NOD/SCID mice, and tumor burden was monitored. The mice were randomized into two groups once the mean tumor volume reached ~75 mm,[3] and mice were administered with KITi (50 mg/kg) or vehicle control (CTL) orally for three weeks. Mice treated with KITi
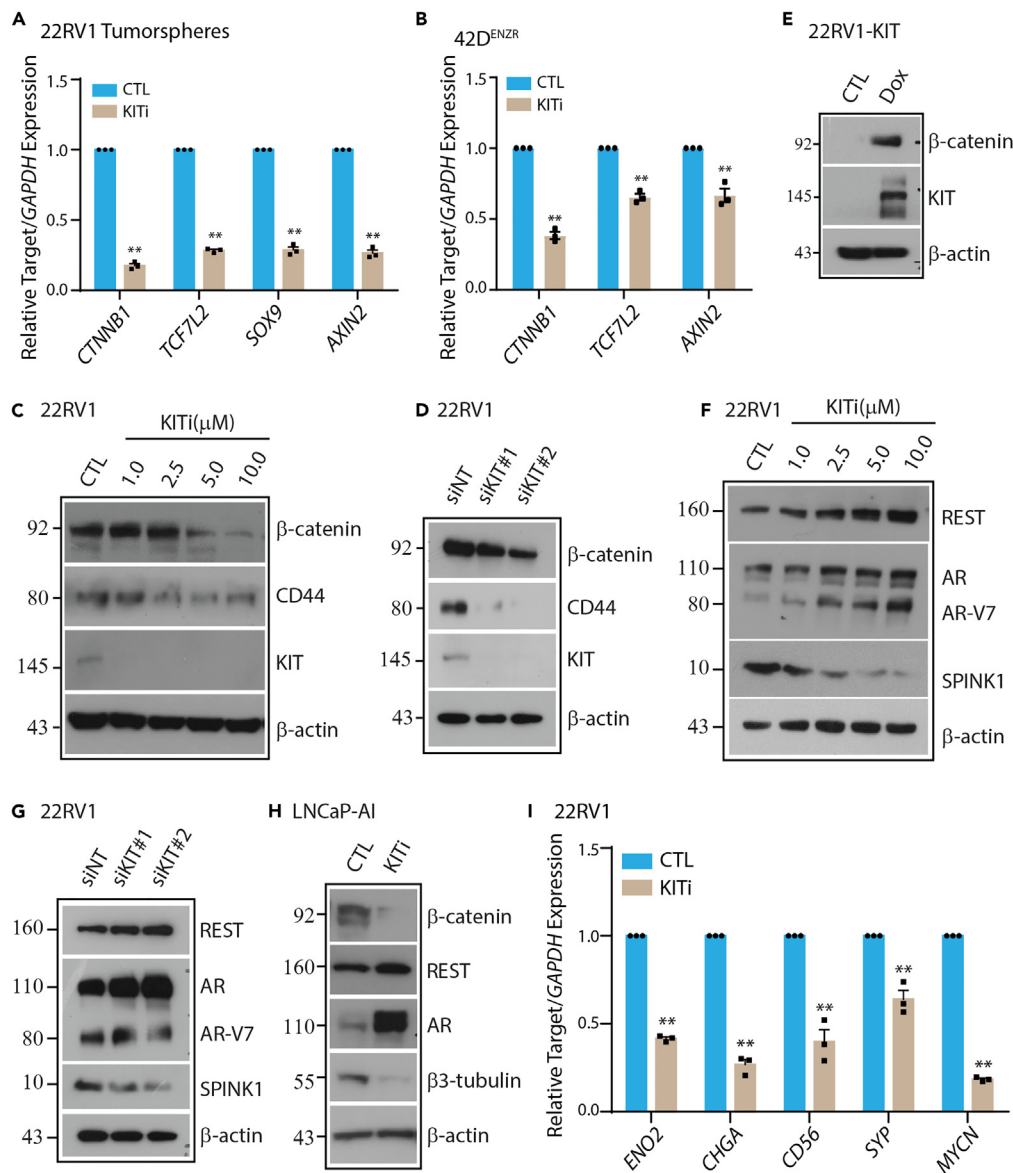
Figure 6. KIT tyrosine kinase inhibition dysregulates the WNT/β-catenin pathway and reinstates AR/REST axis

(A) Bar plot depicting qPCR data for the relative expression of WNT/β-catenin pathway genes in KITi (10 μM)/CTL-treated 22RV1 tumorspheres.

(B) Same as in (A), except for KITi/CTL-treated 42D^{ENZR} cells.

(C) Immunoblot showing the expression level of β-catenin, CD44, and KIT in 22RV1 cells treated with indicated concentrations of KITi and CTL. β-actin was used as the loading control.

(D) Same as in (C), except for *KIT*-silenced 22RV1 cells.

(E) Immunoblot showing β-catenin and KIT levels along with doxycycline (Dox) induction in 22RV1-KIT cells. β-actin was used as loading control.

(F) Immunoblot showing expression level of β-catenin, REST, AR, and β3-tubulin in KITi- (10 μM)/CTL-treated 22RV1 cells. β-actin was used as the loading control.

(G) Same as in (F), except for *KIT*-silenced 22RV1 cells.

(H) Same as in (F), except for KITi- (10 μM)/CTL-treated LNCaP-AI cells.

(I) Bar plot representing qPCR data for the relative expression of NEPC markers using the same cells as in (C). Each experiment was performed in biological triplicates (N = 3); bar represents mean ± SEM, and each dot represents individual value. Statistical significance was calculated using two-way ANOVA followed by Sidak's multiple comparison test. p value: *<0.05 and **<0.01. See also Figure S9.

exhibited diminished tumor growth and ~50% reduction in tumor volume (Figures 7A and 7B). Importantly, KITi treatment showed no adverse effect, as evident by no change in mice body weight between the two groups (Figure 7C). Next, we sought to determine the impact of KITi on tumors excised from xenografted mice by performing IHC for stemness marker CD44 and proliferation marker Ki67. Mice administered with KITi showed significantly decreased levels of CD44 and Ki67 relative to the CTL group (Figures 7D and 7E). Subsequently, we also examined
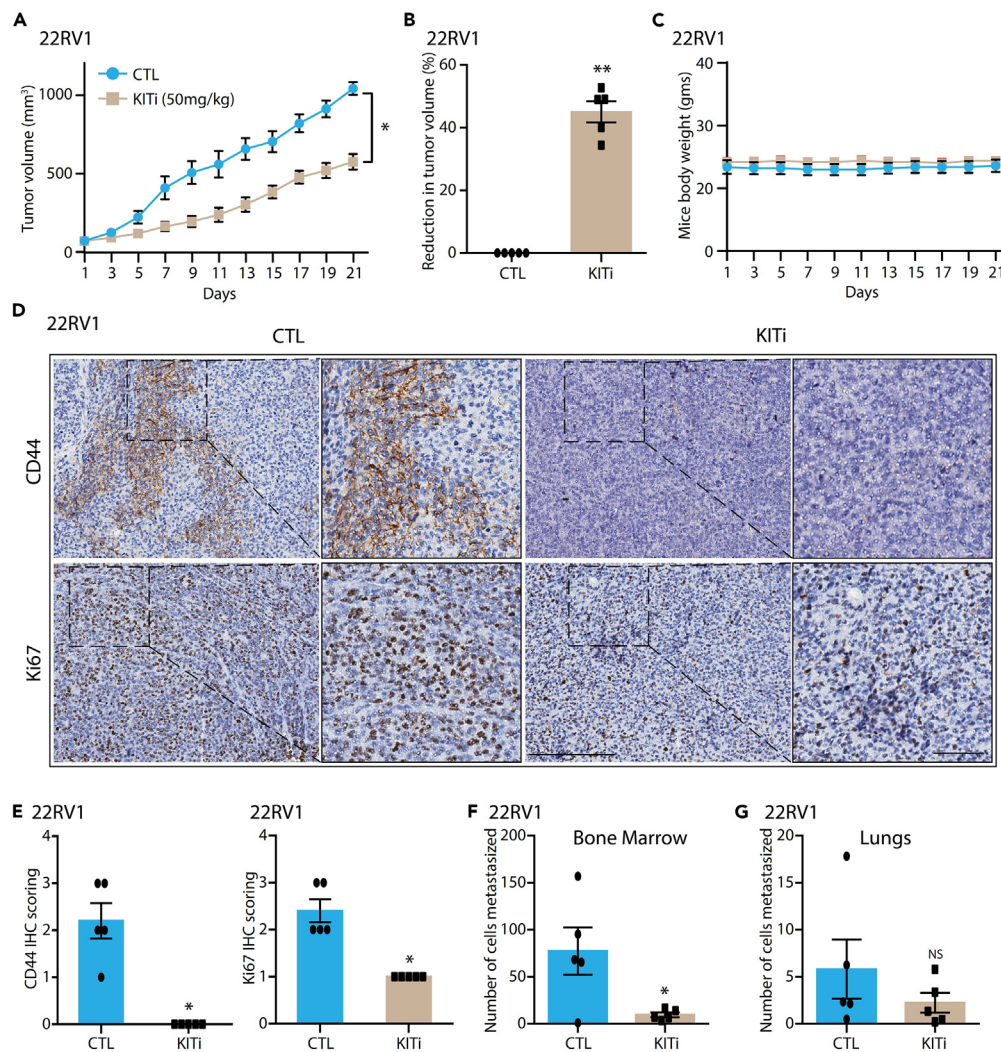
Figure 7. KIT tyrosine kinase inhibition abrogates SPINK1-positive tumor growth and metastases

(A) Line plot representing tumor volume of 22RV1 cells subcutaneously implanted in NOD/SCID mice and administered with KITi (50 mg/kg)/CTL via oral gavage (each group, N = 5).

(B) Bar plot showing the relative percent reduction in tumor volume.

(C) Same as in (A), except for the plot depicting mice's body weight.

(D) Micrographs representing IHC staining for CD44 and Ki67 in tumor sections from xenografted mice as shown in (A). Scale bar represents 200 μm and 50 μm (for insets).

(E) Bar plots showing quantification of IHC staining for CD44 and Ki67. Twenty random fields were quantified for each group.

(F) Bar plots representing the number of cells metastasized to the bone marrow in xenografted mice, as shown in (A).

(G) Same as in (F), except for the number of cells metastasized to the lungs. Bar represents mean ± SEM, and each dot represents individual value. Statistical significance was calculated using unpaired Student's t test. p-value: *<0.05, **<0.01 and NS = non-significant.

the effect of KITi on spontaneous distant metastases and checked the expression of human-specific *Alu* repeats using genomic DNA isolated from the bone marrow and lungs of the mice.[31] KITi-treated mice displayed a reduced number of cells metastasized to distant organs, such as bone and lungs compared with the CTL group (Figures 7F and 7G). These findings summarize the efficacy of pharmacological inhibition of KIT signaling in abrogating SPINK1-mediated prostate tumorigenesis.

DISCUSSION

SPINK1 molecular subtype has been associated with more aggressive disease and overall poor clinical outcomes.[8–11] Earlier, we have shown that AR antagonists alleviate AR- and, its corepressor, REST-mediated transcriptional repression of *SPINK1* in PCa. Moreover, lineage reprogramming factor SOX2 transactivates *SPINK1* during neuroendocrine transdifferentiation, leading to its upregulation.[6,32] A recent study showed that SPINK1 mitigates radiation-induced DNA damage by upregulating EGFR- and Nrf2-dependent antioxidant responses,

subsequently leading to cancer radioresistance.[33] Previously, Ateeq and colleagues demonstrated that SPINK1 interacts with EGFR owing to its structural homology with EGF, and activates downstream signaling cascade, nonetheless they conjectured that EGFR-independent pathways may also be involved in SPINK1-mediated oncogenic effects.[13]

This study deciphers the activation of EGFR-dependent as well as EGFR-independent signaling pathways in SPINK1-positive PCa. Because the EGFR-targeted therapies have demonstrated limited success in metastatic CRPC patients,[34,35] our prime focus was to interrogate the receptor tyrosine kinases, which might function distinctly in androgen-independent prostatic tumors. Different members of the type III receptor tyrosine kinase family, including CSF1R, KIT, FLT3, and PDGFR, exhibited reduced kinase activity upon silencing of SPINK1. Consistent with the impact of ADT on SPINK1, KIT also displayed higher expression post-ADT and an inverse relation with AR signaling, implicating an association of KIT and SPINK1 in CRPC progression.

Because therapeutic targeting of KIT signaling leads to ∼50% reduction in cell proliferation, a pronounced decrease in foci formation, and tumorsphere formation ability, we reasoned the predominant role of KIT in imparting stemness-related attributes, which was validated via the change in the stemness-associated transcription factors and cell surface markers. In line with our findings, KIT is recently shown as a PCa stem cell marker.[24] Besides, the activation and therapeutic potential of KIT-ligand-induced canonical KIT signaling has recently been established in NEPC.[36] These reports confirm the critical role of KIT in lineage plasticity; however, the exact mechanism of KIT signaling and its downstream players remains unexplored in PCa progression.

Our integrated proteome data from SPINK1 knockdown and KIT interactome stipulated mRNA processing, splicing, and translation as some of the commonly altered biological processes. A closer view of the KIT interactome revealed PARP-1, DNA-dependent protein kinase, catalytic subunit (PRKDC), many histones, and hnRNPs as its direct binding partners (Table S1). Concurrently, histones (H1, H2A, H2B, and H4), hnRNPs (HNRNPC, HNRNPK, HNRNPM, HNRNPU), and PRKDC were also reported as PARP1 interacting partners by affinity purification-mass spectrometry.[37] Also, several studies have proven the canonical and non-canonical function of PARP1 in RNA processing, splicing, and translation.[38,39] These findings suggest a plausible role of KIT signaling in tuning RNA metabolism in SPINK1-positive PCa.

We have unraveled β-catenin as a KIT interacting protein, and targeting KIT signaling disrupted the WNT/β-catenin pathway. A previous study in mast cell leukemia has reported similar results, where activated KIT directly interacts with β-catenin and leads to its tyrosine phosphorylation, which triggers its nuclear localization and enhanced transcriptional activity.[40] Moreover, elevated level of β-catenin nuclear localization has been observed in CRPC bone metastases.[41] Our experimental bone metastases mice data also highlighted the role of KIT signaling in bone resorption, where its inhibition resulted in cancellous bone remodeling. These findings demonstrated that the SPINK1-activated KIT kinase modulates β-catenin stability and transactivates target genes in CRPC. Inhibition of KIT signaling concurrently targets the WNT/β-catenin pathway and alleviates stemness-related features in CRPC.

The WNT/β-catenin pathway is known to be modulated by ADT in advanced-stage PCa patients and confers androgen-independent cell survival.[42] The activation of the WNT/β-catenin pathway configures the enzalutamide resistance, and its inhibition resensitizes PCa cells to AR-targeted therapy.[43] Additionally, the CRPC patients with increased β-catenin activity exhibited low AR levels and vice versa,[41] and reciprocal inhibition of β-catenin and AR signaling was observed in prostate tumorigenesis.[44] Similarly, our findings demonstrated that targeting KIT signaling leads to an increase in AR/REST axis, which in turn downregulates SPINK1, leading to the mitigation of neuroendocrine transdifferentiation. Apart from the mutual antagonism between β-catenin and AR signaling, our study also indicates KIT-signaling-mediated proteasomal degradation of AR, which might confer enzalutamide resistance. Overall, our findings demonstrate that inhibition of KIT-signaling-coaxed AR/REST transactivation is of clinical relevance for therapy-resistant CRPC patients, who display activated WNT/β-catenin pathway.

Imatinib, the commonly used type III receptor tyrosine kinase inhibitor, has not delivered any favorable clinical response either as a single agent or in combination therapy for PCa patients.[45–47] Most of these trials have evaluated imatinib's potential as a PDGFR inhibitor due to its high specificity. Therefore, we traversed for a more potent type III receptor tyrosine kinase inhibitor, namely, pexidartinib (PLX3397), which has 10 to 100 times more selectivity for KIT and CSF1R than other related kinases.[48] Our preclinical mice study indicates the therapeutic potential of pexidartinib in abrogating SPINK1-positive CRPC tumor progression. The systemic administration of pexidartinib with AR antagonists may yield better clinical outcomes, particularly in CRPC cases with bone metastasis. Collectively, our findings provide a compelling rationale for therapeutic targeting of KIT signaling either alone or in combination with the mainstay ADT for advanced-stage PCa patients.

Limitations of the study

Our findings suggest that SPINK1 leads to activation of KIT signaling in PCa. Moreover, stimulation of 22RV1 cells with rSPINK1 leads to increase in KIT phosphorylation, and abrogating SPINK1 reduces KIT kinase activity; however, no significant enrichment of SPINK1 peptides was detected in immune complex for KIT pull-down. Considering the secretory nature of SPINK1, whether it directly activates KIT signaling or serves as a non-canonical ligand in PCa needs further exploration. Highly sensitive techniques used to study orphan ligand-receptor interactions such as LRC-TriCEPS can be utilized for deciphering the crosstalk between SPINK1 and KIT.[49]

STAR★METHODS

Detailed methods are provided in the online version of this paper and include the following:

- KEY RESOURCES TABLE
- RESOURCE AVAILABILITY
  - ○ Lead contact

- ○ Materials availability
- ○ Data and code availability
- EXPERIMENTAL MODEL AND STUDY PARTICIPANT DETAILS
  - ○ Prostate cancer patient specimens
  - ○ Cell lines
  - ○ Mice studies
- METHOD DETAILS
  - ○ Androgen deprivation and drug treatment
  - ○ Transient transfection
  - ○ Plasmids and lentiviral packaging
  - ○ Proteome and phosphoproteome profiling
  - ○ Immunoprecipitation followed by mass spectrometry
  - ○ Cytotoxicity assay
  - ○ Cell proliferation and viability assay
  - ○ Foci formation assay
  - ○ Tumorsphere assay
  - ○ Flow cytometry analysis
  - ○ Immunoblot analysis
  - ○ Immunofluorescence staining
  - ○ Quantitative-PCR (QPCR) analysis
  - ○ Immunohistochemistry
  - ○ Micro-computed tomography (μCT)
- QUANTIFICATION AND STATISTICAL ANALYSIS
  - ○ *In silico* analysis

SUPPLEMENTAL INFORMATION

Supplemental information can be found online at https://doi.org/10.1016/j.isci.2024.108794.

AUTHOR CONTRIBUTIONS

N.M. and B.A. conceptualized the study and designed the methodology; N.M., U.K.K., and A.G. conducted the *in vitro* experiments; N.M. and B.A. performed the mice xenograft studies; N.M., U.K.K., A.G., and B.A. did the formal analysis and visualization; N.P. and N.G. assembled and provided the PCa tissue microarrays and related clinical information; S.C. performed the immunohistochemical staining; N.M. and B.A. wrote the original research manuscript; and B.A. supervised and directed the overall project. All authors read and approved the final manuscript.

DECLARATION OF INTERESTS

N.P. is a consultant to Astrazeneca.

REFERENCES

1. Lonergan, P.E., and Tindall, D.J. (2011). Androgen receptor signaling in prostate cancer development and progression. J. Carcinog. 10, 20.

2. Scher, H.I., and Sawyers, C.L. (2005). Biology of progressive, castration-resistant prostate cancer: directed therapies targeting the androgen-receptor signaling axis. J. Clin. Oncol. 23, 8253–8261.

3. Watson, P.A., Arora, V.K., and Sawyers, C.L. (2015). Emerging mechanisms of resistance to androgen receptor inhibitors in prostate cancer. Nat. Rev. Cancer 15, 701–711.

4. Aggarwal, R., Huang, J., Alumkal, J.J., Zhang, L., Feng, F.Y., Thomas, G.V., Weinstein, A.S., Friedl, V., Zhang, C., Witte, O.N., et al. (2018). Clinical and Genomic Characterization of Treatment-Emergent Small-Cell Neuroendocrine Prostate Cancer: A Multi-institutional Prospective Study. J. Clin. Oncol. 36, 2492–2503.

5. Rickman, D.S., Beltran, H., Demichelis, F., and Rubin, M.A. (2017). Biology and evolution of poorly differentiated neuroendocrine tumors. Nat. Med. 23, 1–10.

6. Tiwari, R., Manzar, N., Bhatia, V., Yadav, A., Nengroo, M.A., Datta, D., Carskadon, S., Gupta, N., Sigouros, M., Khani, F., et al. (2020). Androgen deprivation upregulates SPINK1 expression and potentiates cellular plasticity in prostate cancer. Nat. Commun. 11, 384.

7. Vlachostergios, P.J., Puca, L., and Beltran, H. (2017). Emerging variants of castration-resistant prostate cancer. Curr. Oncol. Rep. 19, 32.

8. Tomlins, S.A., Rhodes, D.R., Yu, J., Varambally, S., Mehra, R., Perner, S., Demichelis, F., Helgeson, B.E., Laxman, B., Morris, D.S., et al. (2008). The role of SPINK1 in ETS rearrangement-negative prostate cancers. Cancer Cell 13, 519–528.

9. Faisal, F.A., Kaur, H.B., Tosoian, J.J., Tomlins, S.A., Schaeffer, E.M., and Lotan, T.L. (2019). SPINK1 expression is enriched in African American prostate cancer but is not associated with altered immune infiltration or oncologic outcomes post-prostatectomy. Prostate Cancer Prostatic Dis. 22, 552–559.

10. Johnson, M.H., Ross, A.E., Alshalalfa, M., Erho, N., Yousefi, K., Glavaris, S., Fedor, H., Han, M., Faraj, S.F., Bezerra, S.M., et al. (2016). SPINK1 Defines a Molecular Subtype of Prostate Cancer in Men with More Rapid Progression in an at Risk, Natural History Radical Prostatectomy Cohort. J. Urol. 196, 1436–1444.

11. Leinonen, K.A., Tolonen, T.T., Bracken, H., Stenman, U.H., Tammela, T.L.J., Saramäki, O.R., and Visakorpi, T. (2010). Association of SPINK1 expression and TMPRSS2:ERG fusion with prognosis in endocrine-treated prostate cancer. Clin. Cancer Res. 16, 2845–2851.

12. Ozaki, N., Ohmuraya, M., Hirota, M., Ida, S., Wang, J., Takamori, H., Higashiyama, S., Baba, H., and Yamamura, K.I. (2009). Serine protease inhibitor Kazal type 1 promotes proliferation of pancreatic cancer cells through the epidermal growth factor receptor. Mol. Cancer Res. 7, 1572–1581.

13. Ateeq, B., Tomlins, S.A., Laxman, B., Asangani, I.A., Cao, Q., Cao, X., Li, Y., Wang, X., Feng, F.Y., Pienta, K.J., et al. (2011). Therapeutic targeting of SPINK1-positive prostate cancer. Sci. Transl. Med. 3, 72ra17.

14. Shukla, S., Cyrta, J., Murphy, D.A., Walczak, E.G., Ran, L., Agrawal, P., Xie, Y., Chen, Y., Wang, S., Zhan, Y., et al. (2017). Aberrant Activation of a Gastrointestinal Transcriptional Circuit in Prostate Cancer Mediates Castration Resistance. Cancer Cell 32, 792–806.e7.

15. Chen, F., Long, Q., Fu, D., Zhu, D., Ji, Y., Han, L., Zhang, B., Xu, Q., Liu, B., Li, Y., et al. (2018). Targeting SPINK1 in the damaged tumour microenvironment alleviates therapeutic resistance. Nat. Commun. 9, 4315.

16. Hunter, T. (2000). Signaling—2000 and beyond. Cell 100, 113–127.

17. O'Brien, S.G., Guilhot, F., Larson, R.A., Gathmann, I., Baccarani, M., Cervantes, F., Cornelissen, J.J., Fischer, T., Hochhaus, A., Hughes, T., et al. (2003). Imatinib compared with interferon and low-dose cytarabine for newly diagnosed chronic-phase chronic myeloid leukemia. N. Engl. J. Med. 348, 994–1004.

18. Joensuu, H., Eriksson, M., Sundby Hall, K., Hartmann, J.T., Pink, D., Schütte, J., Ramadori, G., Hohenberger, P., Duyster, J., Al-Batran, S.E., et al. (2012). One vs three years of adjuvant imatinib for operable gastrointestinal stromal tumor: a randomized trial. JAMA 307, 1265–1272.

19. Wiredja, D.D., Koyutürk, M., and Chance, M.R. (2017). The KSEA App: a web-based tool for kinase activity inference from quantitative phosphoproteomics. Bioinformatics 33, 3489–3491.

20. Ulgen, E., Ozisik, O., and Sezerman, O.U. (2019). pathfindR: An R Package for Comprehensive Identification of Enriched Pathways in Omics Data Through Active Subnetworks. Front. Genet. 10, 858.

21. Huang, D.W., Sherman, B.T., and Lempicki, R.A. (2009). Systematic and integrative analysis of large gene lists using DAVID bioinformatics resources. Nat. Protoc. 4, 44–57.

22. Nouruzi, S., Ganguli, D., Tabrizian, N., Kobelev, M., Sivak, O., Namekawa, T., Thaper, D., Baca, S.C., Freedman, M.L., Aguda, A., et al. (2022). ASCL1 activates neuronal stem cell-like lineage programming through remodeling of the chromatin landscape in prostate cancer. Nat. Commun. 13, 2282.

23. Leong, K.G., Wang, B.E., Johnson, L., and Gao, W.Q. (2008). Generation of a prostate from a single adult stem cell. Nature 456, 804–808.

24. Harris, K.S., Shi, L., Foster, B.M., Mobley, M.E., Elliott, P.L., Song, C.J., Watabe, K., Langefeld, C.D., and Kerr, B.A. (2021). CD117/c-kit defines a prostate CSC-like subpopulation driving progression and TKI resistance. Sci. Rep. 11, 1465.

25. Ali, S., and Ali, S. (2007). Role of c-kit/SCF in cause and treatment of gastrointestinal stromal tumors (GIST). Gene 401, 38–45.

26. Gattei, V., Aldinucci, D., Quinn, J.M., Degan, M., Cozzi, M., Perin, V., Iuliis, A.D., Juzbasic, S., Improta, S., Athanasou, N.A., et al. (1996). Human osteoclasts and preosteoclast cells (FLG 29.1) express functional c-kit receptors and interact with osteoblast and stromal cells via membrane-bound stem cell factor. Cell Growth Differ. 7, 753–763.

27. Henry, M.D., Silva, M.D., Wen, S., Siebert, E., Solin, E., Chandra, S., and Worland, P.J. (2005). Spiculated periosteal response induced by intraosseous injection of 22Rv1 prostate cancer cells resembles subset of bone metastases in prostate cancer patients. Prostate 65, 347–354.

28. Goel, S., Bhatia, V., Kundu, S., Biswas, T., Carskadon, S., Gupta, N., Asim, M., Morrissey, C., Palanisamy, N., and Ateeq, B. (2021). Transcriptional network involving ERG and AR orchestrates Distal-less homeobox-1 mediated prostate cancer progression. Nat. Commun. 12, 5325.

29. Wielenga, V.J., Smits, R., Korinek, V., Smit, L., Kielman, M., Fodde, R., Clevers, H., and Pals, S.T. (1999). Expression of CD44 in Apc and Tcfmutant mice implies regulation by the WNT pathway. Am. J. Pathol. 154, 515–523.

30. Lin, H.K., Wang, L., Hu, Y.C., Altuwaijri, S., and Chang, C. (2002). Phosphorylation-dependent ubiquitylation and degradation of androgen receptor by Akt require Mdm2 E3 ligase. EMBO J. 21, 4037–4048.

31. van der Horst, E.H., Leupold, J.H., Schubbert, R., Ullrich, A., and Allgayer, H. (2004). TaqMan®-based quantification of invasive cells in the chick embryo metastasis assay. Biotechniques 37, 940–946.

32. Manzar, N., Ganguly, P., Khan, U.K., and Ateeq, B. (2023). Transcription networks rewire gene repertoire to coordinate cellular reprograming in prostate cancer. Semin. Cancer Biol. 89, 76–91.

33. Suwa, T., Kobayashi, M., Shirai, Y., Nam, J.M., Tabuchi, Y., Takeda, Y., Akamatsu, S., Ogawa, O., Mizowaki, T., Hammond, E.M., and Harada, H. (2021). SPINK1 as a plasma marker for tumor hypoxia and a therapeutic target for radiosensitization. JCI Insight 6, e148135.

34. Pezaro, C., Rosenthal, M.A., Gurney, H., Davis, I.D., Underhill, C., Boyer, M.J., Kotasek, D., Solomon, B., and Toner, G.C. (2009). An open-label, single-arm phase two trial of gefitinib in patients with advanced or metastatic castration-resistant prostate cancer. Am. J. Clin. Oncol. 32, 338–341.

35. Ziada, A., Barqawi, A., Glode, L.M., Varella-Garcia, M., Crighton, F., Majeski, S., Rosenblum, M., Kane, M., Chen, L., and Crawford, E.D. (2004). The use of trastuzumab in the treatment of hormone refractory prostate cancer; phase II trial. Prostate 60, 332–337.

36. Han, M., Li, F., Zhang, Y., Dai, P., He, J., Li, Y., Zhu, Y., Zheng, J., Huang, H., Bai, F., and Gao, D. (2022). FOXA2 drives lineage plasticity and KIT pathway activation in neuroendocrine prostate cancer. Cancer Cell 40, 1306–1323.e8.

37. Isabelle, M., Moreel, X., Gagné, J.P., Rouleau, M., Ethier, C., Gagné, P., Hendzel, M.J., and Poirier, G.G. (2010). Investigation of PARP-1, PARP-2, and PARG interactomes by affinity-purification mass spectrometry. Proteome Sci. 8, 22.

38. Melikishvili, M., Chariker, J.H., Rouchka, E.C., and Fondufe-Mittendorf, Y.N. (2017). Transcriptome-wide identification of the RNA-binding landscape of the chromatin-associated protein PARP1 reveals functions in RNA biogenesis. Cell Discov. 3, 17043.

39. Kim, D.S., Challa, S., Jones, A., and Kraus, W.L. (2020). PARPs and ADP-ribosylation in RNA biology: from RNA expression and processing to protein translation and proteostasis. Genes Dev. 34, 302–320.

40. Kajiguchi, T., Lee, S., Lee, M.J., Trepel, J.B., and Neckers, L. (2008). KIT regulates tyrosine phosphorylation and nuclear localization of

beta-catenin in mast cell leukemia. Leuk. Res. *32*, 761–770.

41. Wan, X., Liu, J., Lu, J.-F., Tzelepi, V., Yang, J., Starbuck, M.W., Diao, L., Wang, J., Efstathiou, E., Vazquez, E.S., et al. (2012). Activation of β-catenin signaling in androgen receptor–negative prostate cancer cells. Clin. Cancer Res. *18*, 726–736.

42. Rajan, P., Sudbery, I.M., Villasevil, M.E.M., Mui, E., Fleming, J., Davis, M., Ahmad, I., Edwards, J., Sansom, O.J., Sims, D., et al. (2014). Next-generation sequencing of advanced prostate cancer treated with androgen-deprivation therapy. Eur. Urol. *66*, 32–39.

43. Zhang, Z., Cheng, L., Li, J., Farah, E., Atallah, N.M., Pascuzzi, P.E., Gupta, S., and Liu, X. (2018). Inhibition of the Wnt/β-Catenin Pathway Overcomes Resistance to Enzalutamide in Castration-Resistant Prostate Cancerβ-Catenin in Enzalutamide Resistance. Cancer Res. *78*, 3147–3162.

44. Patel, R., Brzezinska, E.A., Repiscak, P., Ahmad, I., Mui, E., Gao, M., Blomme, A., Harle, V., Tan, E.H., Malviya, G., et al. (2020). Activation of β-Catenin Cooperates with Loss of Pten to Drive AR-Independent Castration-Resistant Prostate Cancerβ-Catenin Activation Induces AR-Independent CRPC. Cancer Res. *80*, 576–590.

45. Mathew, P., Thall, P.F., Jones, D., Perez, C., Bucana, C., Troncoso, P., Kim, S.J., Fidler, I.J., and Logothetis, C. (2004). Platelet-derived growth factor receptor inhibitor imatinib mesylate and docetaxel: a modular phase I trial in androgen-independent prostate cancer. J. Clin. Oncol. *22*, 3323–3329.

46. Bajaj, G.K., Zhang, Z., Garrett-Mayer, E., Drew, R., Sinibaldi, V., Pili, R., Denmeade, S.R., Carducci, M.A., Eisenberger, M.A., and DeWeese, T.L. (2007). Phase II study of imatinib mesylate in patients with prostate cancer with evidence of biochemical relapse after definitive radical retropubic prostatectomy or radiotherapy. Urology *69*, 526–531.

47. Mathew, P., Pisters, L.L., Wood, C.G., Papadopoulos, J.N., Williams, D.L., Thall, P.F., Wen, S., Horne, E., Oborn, C.J., Langley, R., et al. (2009). Neoadjuvant platelet derived growth factor receptor inhibitor therapy combined with docetaxel and androgen ablation for high risk localized prostate cancer. J. Urol. *181*, 81–87.

48. DeNardo, D.G., Brennan, D.J., Rexhepaj, E., Ruffell, B., Shiao, S.L., Madden, S.F., Gallagher, W.M., Wadhwani, N., Keil, S.D., Junaid, S.A., et al. (2011). Leukocyte complexity predicts breast cancer survival and functionally regulates response to chemotherapy. Cancer Discov. *1*, 54–67.

49. Frei, A.P., Moest, H., Novy, K., and Wollscheid, B. (2013). Ligand-based receptor identification on living cells and tissues using TRICEPS. Nat. Protoc. *8*, 1321–1336.

50. Abida, W., Cyrta, J., Heller, G., Prandi, D., Armenia, J., Coleman, I., Cieslik, M., Benelli, M., Robinson, D., Van Allen, E.M., et al. (2019). Genomic correlates of clinical outcome in advanced prostate cancer. Proc. Natl. Acad. Sci. USA *116*, 11428–11436.

51. Beltran, H., Prandi, D., Mosquera, J.M., Benelli, M., Puca, L., Cyrta, J., Marotz, C., Giannopoulou, E., Chakravarthi, B.V.S.K., Varambally, S., et al. (2016). Divergent clonal evolution of castration-resistant neuroendocrine prostate cancer. Nat. Med. *22*, 298–305.

52. Puca, L., Bareja, R., Prandi, D., Shaw, R., Benelli, M., Karthaus, W.R., Hess, J., Sigouros, M., Donoghue, A., Kossai, M., et al. (2018). Patient derived organoids to model rare prostate cancer phenotypes. Nat. Commun. *9*, 2404.

53. Bishop, J.L., Thaper, D., Vahid, S., Davies, A., Ketola, K., Kuruma, H., Jama, R., Nip, K.M., Angeles, A., Johnson, F., et al. (2017). The master neural transcription factor BRN2 is an androgen receptor–suppressed driver of neuroendocrine differentiation in prostate cancer. Cancer Discov. *7*, 54–71.

54. Jin, S., Guerrero-Juarez, C.F., Zhang, L., Chang, I., Ramos, R., Kuan, C.-H., Myung, P., Plikus, M.V., and Nie, Q. (2021). Inference and analysis of cell-cell communication using CellChat. Nat. Commun. *12*, 1088.

55. Bocchi, R., Egervari, K., Carol-Perdiguer, L., Viale, B., Quairiaux, C., De Roo, M., Boitard, M., Oskouie, S., Salmon, P., and Kiss, J.Z. (2017). Perturbed Wnt signaling leads to neuronal migration delay, altered interhemispheric connections and impaired social behavior. Nat. Commun. *8*, 1158.

56. Bhalla, R., Kunju, L.P., Tomlins, S.A., Christopherson, K., Cortez, C., Carskadon, S., Siddiqui, J., Park, K., Mosquera, J.M., Pestano, G.A., et al. (2013). Novel dual-color immunohistochemical methods for detecting ERG-PTEN and ERG-SPINK1 status in prostate carcinoma. Mod. Pathol. *26*, 835–848.

STAR★METHODS

KEY RESOURCES TABLE

REAGENT or RESOURCE	SOURCE	IDENTIFIER
Antibodies		
KIT	Cell Signaling Technology	Cat#37805; RRID: AB_2799120
phospho-KIT	Cell Signaling Technology	Cat#3073; RRID: AB_1147635
β-catenin	Cell Signaling Technology	Cat#8480; RRID: AB_11127855
CD44	Cell Signaling Technology	Cat# 3570; RRID: AB_2076465
phospho-Akt	Cell Signaling Technology	Cat# 13038; RRID: AB_2629447
total-AKT	Cell Signaling Technology	Cat# 9272; RRID: AB_329827
phospho-ERK	Cell Signaling Technology	Cat# 4377; RRID: AB_331775
total-ERK	Cell Signaling Technology	Cat# 4695; RRID: AB_390779
AR	Cell Signaling Technology	Cat# 5153; RRID: AB_10691711
REST	Abcam	Cat# ab75785; RRID: AB_1310639
β3-tubulin	Cell Signaling Technology	Cat# 5568; RRID: AB_10694505
SPINK1	R&D Systems	Cat# MAB7496-SP
β-actin	Abcam	Cat# ab6276; RRID: AB_2223210
CD44-PE	Miltenyi Biotec	Cat# 130-113-904; RRID: AB_2726395
phospho-EGFR	Abcam	Cat# ab5636; RRID: AB_305005
EGFR	Cell Signaling Technology	Cat# 2232S; RRID: AB_331707
Bacterial and virus strains		
ViraPower™ Lentiviral Packaging Mix	Invitrogen	K4975-00
Biological samples		
Human prostate cancer patients' tissue microarrays	Department of Pathology, Henry Ford Health System, Detroit, MI	NA
Chemicals, peptides, and recombinant proteins		
Pexidartinib (PLX-3397)	MedChemExpress	Cat. No. HY-16749
Recombinant human SPINK1 protein	Abcam	Cat No. ab152041
Protease Inhibitor Cocktail	Genetix	Cat. No. PG-122
Phosphatase Inhibitor Cocktail Set-II	Calbiochem	Cat. No. 524625
Trypsin	Sigma	Cat. No. T4049
Matrigel Matrix	Corning	Cat. No. 354234
TRIzol	Takara	Cat. No. 9108
Opti-MEM	Thermo Fisher Scientific	Cat No. 31985062
Polyethylene glycol-400 (PEG-400)	Sigma	Cat. No. BCBZ4351
Blasticidine	Sigma	Cat. No. 15205
Polyethylenimine	Polysciences	Cat No. 23966
Penicillin-Streptomycin (10,000 U/mL)	Thermo Fisher Scientific	Cat. No. 15140-122
Puromycin	Sigma	Cat No. P8833
Polybrene	Sigma	Cat No.107689
Critical commercial assays		
TaqMan TAMRA probe	Applied Biosystems	Cat. No. 450025
TaqMan Universal PCR Master Mix	Applied Biosystems	Cat. No.4304437
GeneSure First Strand cDNA Synthesis Kit	Genetix	Cat No. PGK162-B

Continued

REAGENT or RESOURCE	SOURCE	IDENTIFIER
GeneSure SYBR Green/ROX qPCR Master Mix	Genetix	Cat. No. PGK022A
Deposited data		
Proteome and phosphoproteome data	Current manuscript	PRIDE consortium (PXD043086)
Metastatic Prostate Adenocarcinoma	Abida et al.[50]	SU2C/PCF Dream Team https://github.com/cBioPortal/datahub/tree/master/public/prad_su2c_2019
Neuroendocrine Prostate Cancer	Beltran et al.[51]	Multi-Institute, Nat Med 2016. https://www.cbioportal.org/study/clinicalData?id=nepc_wcm_2016
Pre- and post-ADT treated PCa specimens	Rajan et al.[42]	GSE48403
NEPC organoids	Puca et al.[52]	GSE112786
Enzalutamide-resistant cell line models	Nouruzi et al.[22]	GSE183199
Single-cell RNA-Seq data	Han et al.[36]	https://ngdc.cncb.ac.cn/(OMIX001928)
Experimental models: Cell lines		
LNCaP	ATCC	Cat#CRL-2876; RRID: CVCL_2235
VCaP	ATCC	Cat#CRL-2505; RRID: CVCL_1045
22RV1	ATCC	Cat#HTB-81; RRID: CVCL_0105
DU145	ATCC	Cat#CRL-1435; RRID: CVCL_0035
PC3	ATCC	Cat#CRL-5813; RRID: CVCL_1576
NCIH660	ATCC	Cat#CRL-3607; RRID: CVCL_3791
RWPE1	ATCC	Cat#; CRL-; RRID: CVCL_2164
PNT2	ATCC	Cat#R70007; RRID: CVCL_6911
HEK293FT	ATCC	Cat# PTA-5077 RRID: CVCL_6911
42D^ENZR	Bishop et al.[53]	MR42D; RRID: CVCL_RW50
Experimental models: Organisms/strains		
NOD/SCID mice (NOD.Cg-Prkdc^Scid/J)	The Jackson Laboratory	JAX: R70007; RRID: IMSR_JAX:001303
Oligonucleotides		
siKIT	Dharmacon	Cat No. LU-003150-00-0002
siNT	Dharmacon	Cat. No. D−001810-10-05
Primers for *GAPDH*, see Table S2	Macrogen	NA
Primers for *MYC*, see Table S2	Macrogen	NA
Primers for *NANOG*, see Table S2	Macrogen	NA
Primers for *OCT4/POU5F1*, see Table S2	Macrogen	NA
Primers for *SOX2*, see Table S2	Macrogen	NA
Primers for *TET1*, see Table S2	Macrogen	NA
Primers for *AURKA*, see Table S2	Macrogen	NA
Primers for *ABCG2*, see Table S2	Macrogen	NA
Primers for *ALDH1A1*, see Table S2	Macrogen	NA
Primers for *CD24*, see Table S2	Macrogen	NA
Primers for *CD44*, see Table S2	IDT	NA
Primers for *KIT*, see Table S2	Macrogen	NA
Primers for *CTNNB1*, see Table S2	Macrogen	NA
Primers for *TCF7L2*, see Table S2	Macrogen	NA

(Continued on next page)

Continued

REAGENT or RESOURCE	SOURCE	IDENTIFIER
Primers for *AXIN2*, see Table S2	Macrogen	NA
Primers for *SOX9*, see Table S2	Macrogen	NA
Primers for *ENO2*, see Table S2	Sigma	NA
Primers for *CHGA*, see Table S2	Sigma	NA
Primers for *CD56/NCAM1*, see Table S2	Sigma	NA
Primers for *SYP*, see Table S2	Sigma	NA
Primers for *ECAD/CDH1*, see Table S2	Macrogen	NA
Primers for *NCAD/CDH2*, see Table S2	Macrogen	NA
Primers for *EPCAM*, see Table S2	IDT	NA
Primers for *SPINK1*, see Table S2	Macrogen	NA
Primers for *SYN1*, see Table S2	Macrogen	NA
Primers for *BDNF*, see Table S2	Macrogen	NA
Primers for Human *ALU*, see Table S2	Macrogen	NA
Software and algorithms		
KSEA App	Wiredja et al.[19]	https://casecpb.shinyapps.io/ksea/
DAVID	Huang et al.[21]	https://david.ncifcrf.gov/summary.jsp
CTVox	Bruker, Belgium	https://www.bruker.com/
CTAn	Bruker, Belgium	https://www.bruker.com/
Flowjo v10.7 software	Becton, Dickinson & Company	https://www.flowjo.com/
GraphPad Prism 6 software	GraphPad Prism Software Inc.	https://www.graphpad.com/
Adobe Illustrator 2017 software	Adobe Systems Inc.	https://www.adobe.com/cn/
CellChat-1.6.1	Jin et al.[54]	https://github.com/sqjin/CellChat
pheatmap-1.0.12	R package	https://rdrr.io/cran/pheatmap/
pathfindR	R package	https://github.com/egeulgen/pathfindR
ggplot2-3.4.3	R package	https://github.com/tidyverse/ggplot2/releases
ImageJ	NIH	https://imagej.nih.gov/ij/

RESOURCE AVAILABILITY

Lead contact

Further information and requests for resources and reagents should be directed to and will be fulfilled by the lead contact, Bushra Ateeq.

Materials availability

This study did not generate new unique reagents or materials.

Data and code availability

- The proteome and phosphoproteome profiles of the 22RV1-shSCRM and 22RV1-shSPINK1 cells are deposited in the PRIDE consortium (PXD043086) and freely accessible. Other publicly available gene expression datasets were downloaded from the cBioPortal, namely: Metastatic Prostate Adenocarcinoma (SU2C/PCF Dream Team, PNAS 2019) and Neuroendocrine Prostate Cancer (Multi-Institute, Nat Med 2016). Other datasets used in the study were retrieved from NCBI GEO, such as GSE48403 for pre- and post-ADT treated PCa specimens, GSE112786 for NEPC organoids and GSE183199 for Enzalutamide-resistant cell line models. The single-cell RNA-Seq data was downloaded from the National Genomics Data Center (https://ngdc.cncb.ac.cn/) with the accession number OMIX: OMIX001928.
- This study does not report any original codes.
- Any additional information required to re-analyze the data reported in this paper will be made available upon request from the lead contact.

EXPERIMENTAL MODEL AND STUDY PARTICIPANT DETAILS

Prostate cancer patient specimens

The tissue microarrays (TMAs) comprising of prostate cancer patients were obtained from the Department of Pathology, Henry Ford Health System, Detroit, MI. The TMAs contain PCa cases with radical prostatectomy, and most of them were localized cancer cases and some with lymph node metastases. All specimens were collected after receiving patient's informed consent and Institutional Review Board approval following the ethical principles instated by Declaration of Helsinki. The TMAs were immunostained for KIT and SPINK1 expression.

Cell lines

The prostate cancer (LNCaP, VCaP, 22RV1, DU145, PC3, NCIH660), the benign prostatic epithelial (RWPE1 and PNT2), and the human epithelial (HEK293FT) cell lines were procured from the American Type Cell Culture (ATCC). They were cultured in their recommended media supplemented with 10% fetal bovine serum (FBS) (Thermo Fisher Scientific) and 0.5% Penicillin-Streptomycin (Pen-Strep) (Thermo Fisher Scientific) following the ATCC guidelines. The enzalutamide-resistant 42D^{ENZR} cell line was generously provided by Prof. Amina Zoubeidi.[53] The authentication of cell lines was performed using short tandem repeat (STR) profiling at the Lifecode Technologies Private Limited, Bangalore and DNA Forensics Laboratory, New Delhi. The cell lines were routinely monitored for any Mycoplasma contamination using the PlasmoTest mycoplasma detection kit (InvivoGen).

Mice studies

The immunodeficient NOD/SCID mice (NOD.Cg-Prkdc^{Scid}/J) were procured from The Jackson Laboratory and were maintained as per their recommended guidelines. All procedures in the mice xenograft studies were implemented in accordance with the guidelines of Institutional Animal Ethics Committee of the Indian Institute of Technology Kanpur, India and approved by the Committee for the Purpose of Control and Supervision of Experiments on Animals (CPCSEA), Ministry of Environment, Forest and Climate Change, Government of India.

METHOD DETAILS

Androgen deprivation and drug treatment

For androgen-independence, LNCaP cells were cultured in the RPMI media without phenol red (Gibco), supplemented with 5% charcoal stripped FBS for 2 weeks. For KITi treatment, cells were serum starved for 6 hrs in the culture media without FBS and then treated with pexidartinib (MedChemExpress, HY-16749) for 60 hrs in complete culture media.

Transient transfection

22RV1 and 42D^{ENZR} cells were seeded at ∼50% confluency and transfected with 30pmol of small interfering RNA (siRNA) against KIT (Dharmacon, Cat No. LU-003150-00-0002) and non-targeting (NT) control (Dharmacon, Cat. No. D−001810-10-05) using X-tremeGENE siRNA transfection reagent (Roche) following the manufacturer's protocol.

Plasmids and lentiviral packaging

The lentiviral pGIPZ plasmids containing short-hairpin RNA (shRNA) such as shScrambled, and shSPINK1 were purchased from Dharmacon (Horizon Discovery Ltd.). Doxycycline-inducible KIT overexpression plasmid (pCLXEBR-pTF-cKit)[55] was a gift from Patrick Salmon (Addgene plasmid #114293). Lentiviral packaging was done using the ViraPower Lentiviral Expression Systems (Invitrogen) following the manufacturer's protocol. Briefly, HEK293FT cells were plated at 90% confluency and transfected with ViraPower packaging mix (9μg) and the lentiviral plasmids (shRNA/overexpression constructs, 3 μg) using Polyethylenimine (Polysciences, 23966). After 60-72 hrs transfection, the lentiviral particles were harvested and stored at −80°C. To produce stable cell line, cells were infected with the lentiviral particles and polybrene (hexadimethrine bromide; 8 μg/mL) (Sigma-Aldrich, 107689). After 24 hrs of infection, the culture media was changed and the shRNA stable cells were selected in puromycin (Sigma-Aldrich, P8833) and Dox-inducible KIT overexpressing cells in blasticidine (Sigma-Aldrich, 15205).

Proteome and phosphoproteome profiling

Cell lysis and protein estimation

22RV1-shSPINK1 and 22RV1-shSCRM cells were washed with 1X phosphate buffered saline (PBS) twice and lysed in hot boiling SDS lysis buffer (5% SDS, 50 mM Tris pH 8.5). The lysate was immediately heated for 5 min and sonicated; then centrifuged at 18000 rpm for 15 min. The supernatant was collected and the protein estimation was done using BCA. 5mg/mL concentrated protein lysate was prepared for each sample and stored in −80°C till further processing.

Sample preparation for mass spectrometry

1mg of protein sample was used for digestion; reduced with 5mM tris(2-carboxyethyl)phosphine (TCEP) and alkylated with 50mM iodoacetamide and further digested with Trypsin (1:50) for 16 hrs at 37°C. Salt was removed using C18 silica cartridge and digested peptides were dried using a speed vac and resuspended in buffer A (2% acetonitrile, 0.1% formic acid). 500μg peptides were used for phosphopeptides enrichment, while 50μg of protein sample was used for digestion in proteome profiling.

Mass spectrometric analysis

All the processed samples were subjected to an EASY-nLC 1000 Liquid Chromatograph (Thermo Fisher Scientific) system coupled with an Orbitrap Exploris (Thermo Fisher Scientific) Mass Spectrometer. 1μg of peptide sample were loaded on C18 column 15cm, 3.0μm Acclaim PepMap (Thermo Fisher Scientific) and separated with 0–40% gradient of buffer B (80% acetonitrile, 0.1% formic acid) at 300nL/min flow rate); LC gradients were run for 110 min. MS1 spectra was acquired with (Max IT = 60ms, AGQ target = 300%; RF Lens = 70%; R = 60K, mass range = 375–1500; Profile data). Dynamic exclusion was employed for 30s and MS2 spectra was acquired for top 20 peptides with MS2 (Max IT = 60 ms, R = 15K, AGC target 100%). For proteome profiling, MS1 spectra was acquired with (Max IT = 25ms, AGQ target = 300%; RF Lens = 70%; R = 60K, mass range = 375–1500; profile data).

Data processing

All samples were processed and raw files containing mass/charge values were created for each sample. These raw files were analyzed against UniProt Human Proteome Reference through Proteome Discoverer Software (v2.5, Thermo Fisher Scientific). For SEQUEST and MS Amanda search, the precursor (10ppm) and fragment mass tolerance (0.02Da) were set. The enzyme specificity for trypsin/P (cleavage at the C-terminus of "K/R: unless followed by "P") and maximum two missed cleavages were considered. Carbamidomethyl at cysteine as fixed; and phosphorylation at S, T and Y, oxidation at methionine, and acetylation at N-terminus both were set as variable modifications. The 0.01 false discovery rate (FDR) was considered for both peptide spectrum match and protein. For proteome profiling, phosphorylation at S, T and Y were not considered as variable modifications.

Immunoprecipitation followed by mass spectrometry

Dox-induced 22RV1-KIT cells were washed with ice-cold PBS twice and lysed with ice-cold lysis buffer (50mM Tris-HCl pH-8.0, 100mM NaCl, 2% NP-40, 2% Triton X-100, 2mM EDTA). The cell lysate was kept on rotation for 60 min at 4°C and then precleared with 100μL Protein A/G PLUS-Agarose bead slurry for 30 min at 4°C. 10% of the precleared lysate was saved as input and the remaining is divided into two equal halves: one with KIT (CST) and the other with Rabbit IgG Isotype control (Invitrogen), incubate them with rotation overnight at 4°C. Protein A/G PLUS-Agarose were washed in the lysis buffer, then added to KIT and IgG containing lysates, and incubated for 4 hrs with rotation at 4°C. The bead-antibody-protein complexes were washed thrice in wash buffer (10mM Tris-HCl pH-7.4, 150mM NaCl, 1% Triton X-100, 2mM EDTA). Elution was done by heating the bead-antibody-protein complex in 2X SDS loading dye without reducing agent for 10 min at 75°C.

Mass spectrometry analysis −50 μg of protein was used for trypsin digestion and the sample preparation and processing for mass spectrometry was done similar to the 22RV1-shSPINK1/22RV1-shSCRM proteome profiling. MS1 spectra was acquired with (Max IT = 25 ms, AGQ target = 300%; RF Lens = 70%; R = 60K, mass range = 375–1500; profile data). Dynamic exclusion was employed for 30s and MS2 spectra was acquired for top 12 peptides with MS2 (Max IT = 22 ms, R = 15K, AGC target 200%). The RAW files generated from IP-MS samples were analyzed against the UniProt Human Proteome Reference through Proteome Discoverer Software (v2.5, Thermo Fisher Scientific). For SEQUEST and MS Amanda search, the precursor (10 ppm) and fragment mass tolerances (0.02 Da) were set. The enzyme specificity for trypsin/P (cleavage at the C-terminus of "K/R: unless followed by "P") was set. Carbamidomethyl at cysteine as fixed and oxidation at methionine and acetylation at N-terminus were set as variable modifications. The 0.01 FDR was considered for both peptide spectrum match and protein.

Cytotoxicity assay

To evaluate the half-maximal inhibitory concentration (IC50) of pexidartinib (KITi), 22RV1 (3 × 10³) cells were seeded in 96-well culture dishes and treated with different concentrations of KITi for 48 hrs. After treatment, Cell Proliferation Reagent WST-1 (Roche) was added and the IC50 was determined following the manufacturer's protocol.

Cell proliferation and viability assay

22RV1/42D^ENZR (3 × 10³) cells were seeded in 96-well culture dishes and treated with different concentrations of pexidartinib (KITi) against DMSO (CTL) in the recommended complete media and incubated for the specified time points (up to 4 days). KITi/CTL containing media was changed after every 48 hrs. At the endpoint, Cell Proliferation Reagent WST-1 (Roche) was added and cell viability was determined following the manufacturer's protocol.

Foci formation assay

22RV1/42D^ENZR (2 × 10³) cells were plated in 6-well culture dishes along with the recommended media and 5% fetal bovine serum (Invitrogen). The KITi treatment was started 2 days after seeding cells and media was changed after every 48 hrs. The assay was terminated after 2 weeks and the foci were fixed with 4% paraformaldehyde (in 1X PBS) and stained with crystal violet solution (0.05% w/v, 20% ethanol and 1X PBS). For quantitation, 10% glacial acetic acid was used for destaining and the absorption was measured at 550nm. The representative images were captured using Leica DFC310 FX microscope (Leica Microsystems).

Tumorsphere assay

22RV1 (1×10^4) cells were seeded in ultra-low attachment 6-well culture dishes in DMEM-F12 media (1:1, Invitrogen) along with EGF (20 ng/mL, Invitrogen), FGF (20 ng/mL, Invitrogen), B27 (1X, Invitrogen) and kept at 37°C and 5% CO_2. After every 2 days, tumorspheres were collected, disintegrated into single cell suspension and re-plated in fresh media along with KITi/CTL. The tumorspheres were harvested after two weeks and the tumorsphere formation efficiency was determined by evaluating the number of spheres >50µm in diameter and the area of tumorspheres were calculated using ImageJ. The representative images were captured using Axio Observer Z1 inverted microscope (Carl Zeiss).

Flow cytometry analysis

For stem cell surface marker staining, KITi/CTL treated 22RV1 (1×10^6) cells were stained with 1:50 dilution of CD44-PE antibody (Miltenyi Biotec, 130-113-904) and incubated for 1 hr at 4°C. The stained population of cells were analyzed by flow cytometry and live cells were gated using forward scatter (FSC) and side scatter (SSC) dot plot. The cells positive for CD44-PE staining were analyzed relative to the respective IgG isotype control. About 1×10^5 events were acquired for each sample on BD FACS Melody Cell Sorter and analyzed with FlowJo version 10.7.

Immunoblot analysis

Cells were washed in ice-cold PBS and protein was extracted using radioimmunoprecipitation assay (RIPA) lysis buffer, supplemented with Protease Inhibitor Cocktail (Genetix) and Phosphatase Inhibitor Cocktail Set-II (Calbiochem). The samples were prepared in Laemmli sample buffer, resolved on SDS-PAGE and transferred to polyvinylidene difluoride (PVDF) membrane (PALL). The membrane was blocked using 5% non-fat dry milk in tris-buffered saline with 0.1% Tween 20 (TBST) for 1 hr at room temperature, and incubated overnight at 4°C with the respective primary antibody: 1:1000 diluted KIT (CST, 37805), 1:1000 diluted phospho-KIT (CST, 3073), 1:1000 diluted EGFR (CST, 2232S), 1:1000 diluted phospho-EGFR (Abcam, ab5636), 1:3000 diluted β-catenin (CST, 8480), 1:1000 diluted CD44 (CST, 3570), 1:1000 diluted phos-pho-Akt (CST, 13038), 1:1000 diluted total-AKT (CST, 9272), 1:1000 diluted phospho-ERK (CST, 4377), 1:1000 diluted total-ERK (CST, 4695), 1:1000 diluted AR (CST, 5153), 1:2000 diluted REST (Abcam, ab75785), 1:1000 diluted β3-tubulin (CST, 5568), 1:500 diluted SPINK1 (R&D Systems, MAB7496-SP), and 1:5000 diluted β-actin (Abcam, ab6276). The blots were then washed thrice in 1X TBST buffer and incubated with the respective horseradish peroxidase-conjugated anti-rabbit/anti-mouse antibody (Jackson ImmunoResearch, 711-035-150 or 711-035-152) for 2 hrs at room temperature. The blots were then washed thrice in TBST, incubated with SuperSignal West Chemiluminescent Substrate (Thermo Fisher Scientific) and the signals were captured using X-ray films.

Immunofluorescence staining

Cells were cultured in the specified conditions on 12mm coverslips in the 24-well culture dishes. The cells were fixed with 4% paraformalde-hyde in PBS, washed with PBS, and permeabilized using PBS with 0.3% Triton X-100 for 10 min. The blocking was done using 5% normal goat serum in PBS along with 0.05% Tween 20 (PBST) for 2 hrs at room temperature. The cells were then incubated with 1:100 diluted CD44 (CST, 3570) primary antibody in PBST overnight at 4°C. Cells were washed thrice using PBST, followed by incubation with 1:600 diluted Alexa Fluor 555 conjugated anti-mouse secondary antibody (CST, 4409) in PBST for 1 hr at room temperature. Cells were washed in PBST and then stained with DAPI (Sigma-Aldrich). The coverslips were mounted with VECTASHIELD antifade mounting medium (Vector laboratories) on glass slides and sealed with nail polish to prevent drying. The representative images were captured using Axio Observer Z1 motorized inverted fluores-cence microscope (Carl Zeiss).

Quantitative-PCR (QPCR) analysis

The total RNA was extracted using RNAiso Plus (Takara) and 1µg of total RNA was used as template for cDNA synthesis using First Strand cDNA Synthesis Kit (Genetix) following the manufacturer's protocol. For qPCR analysis, each reaction was set up using cDNA template, SYBR Green qPCR Master Mix (Genetix) and the respective primer set (Table S2). The qPCR reactions were performed in triplicates on StepOne Real-Time PCR System (Applied Biosystems) and the relative target gene expression was determined using the ΔΔCt method. List of the primers used is provided in the Table S2.

Immunohistochemistry

Slides were incubated at 60°C for at least 2 hrs and then placed in EnVision FLEX Target Retrieval Solution, either low pH (Agilent DAKO, K800521-2) or high pH (Agilent DAKO, K800421-2) in a PT Link instrument (Agilent DAKO, PT200) at 75°C, heated to 97°C for 20 min, and then cooled to 75°C. Next, slides were washed in 1X EnVision FLEX Wash Buffer (Agilent DAKO, K800721-2) for 5 min. Slides were treated with Peroxidazed 1 (Biocare Medical, PX968M) for 5 min and Background Punisher (Biocare Medical, BP974L) for 10 min with a wash of 1X EnVision FLEX Wash Buffer for 5 min after each step. 1:100 diluted SPINK1 [4D4] (Novus Biologicals, H00006690-M01), 1:20 diluted CD117/KIT (DAKO, A4502), 1:25 diluted CD44 (DAKO, M7082), Ki67 [MIB-1] (DAKO, IR626) in EnVision FLEX Antibody Diluent (Agilent DAKO, K800621-2) was added to each slide and incubated overnight at 4°C. Slides were then washed in 1X EnVision Wash Buffer for 5 min and incubated in either Mach2 Doublestain 1 (Biocare Medical, MRCT523L) (rabbit) or Mach2 Doublestain 2 (Biocare Medical, MRCT525L) (mouse) for 30 min at room temperature in a humidifying chamber. Next, slides were rinsed in 1X EnVision Wash Buffer thrice for 5 min each and treated with a Betazoid DAB solution (Biocare Medical, BDB2004L) for 5 min. Slides were rinsed twice in distilled water,

and treated with EnVision FLEX Hematoxylin (Agilent DAKO, K800821-2) for 5 min. After several rinses in tap water and drying, slides were dipped in xylene approximately 15 times. EcoMount (Biocare Medical, EM897L) was added to each slide, which was then cover slipped.

IHC staining analysis

The scoring for SPINK1 IHC staining was considered as either positive or negative as has been mentioned previously.[56] The scoring for KIT IHC staining was categorised as either: high, medium, low, or negative, based upon the intensity. For the xenograft model, 5 fields were randomly selected from each tumor tissue and the IHC scoring was categorised as follows: 0 (negative), 1 (weak), 2 (moderate), and 3 (strong), based upon the intensity.

Micro-computed tomography (μCT)

The scanning analysis of the tibiae were performed using the micro-CT system SkyScan (Bruker, 1172). The parameters considered for scanning were as follows: 7μm resolution, 48kV voltage, 204μA current and 0.5μm Al filter. The pixel settings were medium with 48kV voltage and 204μA current along with 0.4 rotation step; each sample was scanned in 28min.

The CTVox software was used for 3D visualization and CTAn software for 3D image processing and bone morphometric analysis.

QUANTIFICATION AND STATISTICAL ANALYSIS

In silico analysis

The cut-off for differential expression of proteins and phosphopeptides were: $\log_2$Fold change <-0.6 for downregulated and >0.6 for upregulated, p-value <0.05. The kinase-substrate enrichment analysis was performed using KSEA App.[19] The enrichment of biological processes was done using DAVID functional annotation tool.[21] The correlation of *KIT*, *SPINK1* and *INSR* expression with AR signaling score and NEPC score were analyzed for Metastatic Prostate Adenocarcinoma (SU2C/PCF Dream Team, PNAS 2019[49]) using cBioPortal. The heatmaps were generated using pheatmap (version 1.0.12) package, volcano plots using ggplot2 package and pathway enrichment using pathfindR[20] in R 4.2.1. The publicly available scRNA-seq dataset of NEPC mice models was downloaded as pre-processed raw data and analyzed.[36] Briefly, cell-cell communication analysis was done using CellChat-1.6.1 of the R package. Pathways were annotated using CellChatDB.mouse (http://www.cellchat.org/cellchatdb/), communication probability and network centrality scores were computed by "computeCommunProb" and "netAnalysis_computeCentrality" respectively; plots were visualized using ggplot2-3.4.3.

Statistical analysis

Data are represented as the mean $\pm$ SEM. Statistical significance was measured using GraphPad Prism 6 with the following tests: One-way ANOVA, two-way ANOVA, unpaired two-tailed Student's t-test along with the multiple comparison analysis or otherwise indicated in the respective figure legend. The comparison between the groups was considered significant if p-value <0.05; and indicated as follows: *p < 0.05 and **p < 0.01. All the experiments were conducted in replicates and the error bars denote the standard error of mean (SEM) of at least three independent replicates.